LINKING FOREST CARBON SEQUESTRATION, CO_2 FLUX, AND CLIMATE: 20 YEARS OF EDDY COVARIANCE DATA FROM THE HOWLAND FOREST, MAINE

By Aaron Teets

B.S. Virginia Tech – Blacksburg, VA 2008

A THESIS

Submitted in Partial Fulfillment of the

Requirements for the Degree of

Master of Science

(in Forest Resources)

The Graduate School

University of Maine

December 2016

Advisory Committee:

Shawn Fraver, Assistant Professor of Forest Ecosystems, Advisor

David Hollinger, Director of USDA Northeast Regional Climate Hub

Robert S. Seymour, Curtis Hutchins Professor of Forest Resources

Aaron Weiskittel, Associate Professor of Forest Biometrics and Modeling

LINKING FOREST CARBON SEQUESTRATION, CO_2 FLUX, AND CLIMATE: 20 YEARS OF EDDY COVARIANCE DATA FROM THE HOWLAND FOREST, MAINE

By Aaron Teets

Thesis Advisor: Dr. Shawn Fraver

An Abstract of the Thesis Presented
in Partial Fulfillment of the Requirements for the
Degree of Master of Science
(in Forest Resources)
December 2016

Forest productivity is known to vary in response to annual fluctuations in climate. By assessing how closely forest productivity tracks climate on an annual basis, we can gauge climate sensitivity for a given location. However, our understanding of forest productivity is limited, in part, by the complex methods needed to measure annual stand-level productivity. The eddy covariance technique, whereby CO_2 exchange (flux) is continuously measured at the canopy-atmosphere interface, has clarified our understanding of stand-level carbon dynamics by addressing productivity and its response to climate fluctuations. Biometric approaches, where forest productivity is estimated from the annual growth of individual trees, can offer a more economical alternative to continuous CO_2 flux measurements, while providing annual estimates of CO_2 assimilation. However, attempts to link these measurements of productivity (i.e., CO_2 flux and tree growth) have produced inconsistent results and demonstrated a need for further research.

Using long-term forest inventory data paired with tree-ring data from a mixed-species conifer forest at the Howland Research Forest, central Maine, we developed annual estimates of productivity at species- and stand-levels. We used annual carbon mass increment (derived from tree-ring data and species-specific wood densities) per unit area

as a measure of productivity because it allows direct comparisons with CO_2 flux data. Our results demonstrated strong correlations between carbon mass increment and annual CO_2 flux measurements summarized from previous-year fall to current-year fall, an improvement from calendar year summaries. Further, our results suggest tree growth was lagged one year behind CO_2 flux (i.e., assimilated CO_2 was not allocated to growth until the following year) for about the first half of the time-series, but later became synchronized with current year assimilation. We suspect the shift to synchrony reflects the onset of above-average spring temperatures, which shifted carbon allocation from storage to current-year wood formation.

We also explored the use of annual carbon mass increment as an alternative to traditional standardized tree-ring chronologies for assessing climate–growth relationships. Our approach allowed us to assess these relationships across three levels of organization: individual tree-, species-, and stand-levels. We believe this approach is preferable in complex mixed-species forests, as it provides insights unavailable from the traditional standardization approach, which is restricted to the species level. Our results demonstrated that stand-level growth was sensitive to a different set of climate variables than those affecting individual species. We documented previous summer precipitation (higher better) and spring temperature (warmer better) as the most influential variables affecting stand-level growth at Howland Forest. We conclude the use of carbon mass increment has a broad range of applications within studies of forest productivity, and we suggest that future studies using tree-ring data consider the potential benefits of converting to carbon-mass increment. The following thesis highlights the benefits of implementing annual carbon mass increments for the purpose of addressing a broad range of research questions.

ACKNOWLEDGEMENTS

There are many individuals who have contributed to the successful completion of this research. Foremost, I would like to thank my committee; Shawn Fraver, David Hollinger, Robert Seymour, and Aaron Weiskittel for their encouragement and guidance. I would also like to thank my family for their support throughout the process, and my fellow graduate students as well as roommates for their help during the different phases of this research.

A very sincere thank you to the Howland staff, particularly Holly Hughes and John Lee for logistical support and detailed safety meetings. Long-term data used for this project was made possible thanks to additional support from Andrew Richardson and Bob Evans. Fieldwork was completed with help from many contributors; in particular thanks to Emily Anderson, Nathan Wesley, Danae Shurn, and Nate Lawrence. Thanks to Hunter Manley, and Jack Clarke for other assistance and companionship at Howland. A special thanks goes to Dave Carter who provided guidance during the early stages.

I would also like to thank the School of Forest Resources, Maine Agricultural and Forest Experiment Station (MAFES), USDA Forest Service, and AmeriFlux Network for providing financial support and making this research possible. I am very thankful for opportunities to attend national meetings and build the skills needed to complete this thesis, and disseminate the results (North American Dendroecological Fieldweek, Association of American Geographers Conference, and AmeriFlux Meeting). Lastly, the Northeastern Wilderness Trust is owed a big thanks for acquiring and protecting Howland Forest, a special place and invaluable resource for ecosystem science.

TABLE OF CONTENTS

LIST OF TABLES

LIST OF FIGURES

PROLOGUE

The emissions from fossil fuel use have increased global atmospheric carbon dioxide (CO_2) concentrations and changed the chemistry of earth's atmosphere. Many researchers are trying to find ways to mitigate the effects of the changing atmospheric CO_2 concentrations. Increasing or maintaining forest productivity is one way to mitigate the effects of climate change by offsetting carbon emissions from burning fossil fuels (Malmsheimer et al. 2008). From 2000-2007, forests sequestered 4.0 $\pm$ 0.7 Pg C of the 8.7 $\pm$ 0.8 Pg C / year in global carbon emissions from fossil fuels and land-use change (Pan et al. 2011). The extent to which forest management could further enhance carbon sequestration is still largely uncertain, partly due to a lack of consistent long-term forest productivity data. Understanding factors that could accelerate or suppress carbon sequestration would improve our ability to model forest contributions to CO_2 sequestration in a changing climate.

Forested ecosystems function as biological carbon sinks by assimilating and storing atmospheric carbon in plant biomass and soils (Grace 2004). The net mass of the carbon molecules converted to plant biomass per unit time and area is used as a measure of forest productivity. Forest carbon pools are dominated by biomass stored in plants, detritus, and soils. The loss of carbon from pools to the atmosphere is considered a carbon source (e.g. decomposition). We can monitor forest productivity using field measurements to track the mass change within carbon pools. The transfer of carbon from one pool to another is considered the carbon flux; we estimate the flux by quantifying the change in carbon pools over time.

Associations between forest age and productivity are commonly used to infer the production efficiency of different forest systems. Net carbon sequestration after a large-scale disturbance may take >15 years to change from a carbon source (to the atmosphere)

to a net carbon sink (Fahey et al. 2005). Following the source phase, rapid regeneration of many young trees results in a high initial rate of sequestration (Bormann and Likens 1979). After the rapid growth phase forests are assumed to follow a decreasing trend of sequestration as they reach maturity (Gough et al. 2008; Amiro et al. 2010; Bradford and Kastendick 2010). Although total ecosystem carbon sequestration rates are expected to decrease as forested ecosystems reach old-age (Pregitzer and Euskirchen 2004), forests continue to be net carbon sinks by accumulating soil and deadwood stores instead of reaching a theoretical equilibrium (Harmon 2001; Luyssaert et al. 2008). Recent studies demonstrating larger trees sequester more carbon than smaller trees (Stephenson et al. 2014), and complex forests becoming larger carbon sinks as they age (D'Amato et al. 2011; Foster et al. 2014) may alter our perspective of old forest carbon dynamics.

By combining forest inventory data, tree-ring reconstructions of productivity over time, and long-term eddy-flux data, this study offers a perspective of carbon dynamics from Howland Research Forest, a mature, mixed-species forest in central Maine, USA. Previous work reveals that the Howland forest has shown an increasing trend in carbon sequestration from 1996-2010 (Keenan et al. 2013). It remains a persistent carbon sink as a multi-strata forest with trees in excess of 300-years old. This site has a species composition similar to that of other forests of the region; as such, it could serve as a surrogate for other managed stands as they reach advanced developmental stages. We use this system to improve our understanding of forest carbon dynamics by quantifying and reporting the landscape-level carbon stocks stored in living trees, the magnitude of annual carbon sequestration using two concurrent methodologies, and the influence of climate on tree growth.

CHAPTER 1 : LINKING FOREST CARBON SEQUESTRATION WITH ANNUAL CO_2 FLUX

1.1 Introduction

Forests play an essential role in the global carbon cycle by removing CO_2 from the atmosphere and storing it in tree biomass. Concerns over elevated atmospheric CO_2 levels have called for a better understanding of factors that influence tree biomass production, including sources of annual variability. At the level of forest stands, annual forest productivity is estimated primarily by tree growth (i.e., carbon assimilated to woody tissue) or eddy covariance (i.e., CO_2 exchange between forest canopies and the atmosphere) measurements. Previous attempts to link these two measurements of forest productivity have yielded inconsistent results (Delpierre et al. 2016), perhaps due to yearly lags between atmospheric CO_2 assimilation and structural growth (Gough et al. 2009). Discrepancies between the two could also result from varying carbon allocation strategies, in particular differential allocation to non-structural carbohydrates (storage for future use) vs. biomass production (structural growth) (Barford et al. 2001; Babst et al. 2013). The simultaneous use of tree-growth and eddy-covariance methods – particularly using lengthy time series – to further evaluate carbon allocation strategies would shed much light on the forest carbon cycle.

Tree growth is regularly inventoried for commercial forestry and ecological studies using repeated diameter measurements of sample trees. These repeated measurements can be used to estimate net primary productivity in any forest type (Clark et al. 2001). However, repeated tree measurements can be time intensive and costly. An alternative to repeated measurements in temperate and boreal systems is utilizing annual tree-ring records (derived from increment cores) to reconstruct previous tree diameters (Bakker 2005). Annual diameter growth can then be converted to biomass growth by using

published allometric equations. This method has the potential to track annual stand-level forest productivity back decades, and more importantly does not require repeated field inventories.

Stand-level forest productivity can also be estimated using the eddy covariance (flux) technique (Baldocchi et al. 1988). Flux towers constructed above tree canopies continuously measure net CO_2 exchange at the canopy-atmosphere interface, with a footprint (i.e., detection radius) ranging from hundreds of meters to several kilometers (Baldocchi 2003). The method utilizes turbulent air currents (eddies) to measure the exchange of CO_2 and other chemicals between ecological communities and the atmosphere. These exchanges are compiled to provide robust datasets capable of tracking year-to-year variability in forest productivity. As these datasets become more temporally robust, researchers can use flux records to track entire forest response to climate variability (Hollinger et al. 2004; Wharton and Falk 2016) and disturbance (Ueyama et al. 2011; Hicke et al. 2012), and to improve ecosystem carbon models (Richardson et al. 2010). However, establishing and maintaining eddy flux towers requires sizeable financial investment and creates many logistical challenges. As a result, flux sites are few in number, which limits the assessment of spatial variability in annual carbon flux. Naturally, we are led to ask if an analogous technique for estimating annual stand-level productivity, such as tree-ring analyses, could be used to clarify our understanding of forest carbon dynamics, including year-to-year associated variability.

Several previous studies have combined the two metrics of productivity – eddy flux and tree-ring methods – to gain a more holistic view of carbon dynamics, yet critical gaps exist in our understanding of how these two metrics are linked on annual timescales. Eddy flux coupled with tree growth has been used to validate photosynthesis and transpiration rates (Catovsky et al. 2002) and to evaluate forest productivity response to climate (Grant

et al. 2009; Wharton and Falk 2016). Previous attempts to link year-to-year flux estimates with radial growth (Rocha et al. 2006; Zweifel et al. 2010) and carbon mass increment (Babst et al. 2013; Delpierre et al. 2016) have produced inconsistent results and thus call for additional research. Babst et al. (2013) demonstrate positive correlations between carbon increment and early season flux measurements (January-July), yet Delpierre et al. (2016) suggest the two metrics are uncorrelated on an annual basis.

The discrepancies between year-to-year tree growth and eddy flux measurements are likely due to temporary non-structural carbohydrate storage (Gough et al. 2009; Babst et al. 2013; Delpierre et al. 2016). Plants accumulate non-structural carbohydrates (primarily sugars and starch) via photosynthesis that can be mobilized and used for later growth or other plant functions (Chapin et al. 1990). Non-structural carbohydrates are critical for dormant season respiration and maintenance, and unused carbohydrates will often contribute to early season structural growth in the following season (Keel et al. 2006; Elgin et al. 2010; Mitchelot et al. 2011). Non-structural carbohydrate stores can last for several years; in some species they can remain in stemwood for over a decade (Richardson et al. 2013). As a result of carbohydrate storage, multi-year metrics of carbon mass increment, when compared to annual carbon mass increment, appear to be more strongly correlated with carbon flux data (Barford et al. 2001; Gough et al. 2008).

The specific objective of this study was to characterize the year-to-year relationship between carbon mass increment (from tree ring series) and annual carbon flux (from eddy covariance measurements). We assessed how annual carbon sequestration changed over time using a mixed-species, multi-aged forest as our study system. We expect this study to provide a framework for tracking annual carbon sequestration using dendrochronological methods that can be used in future studies. Our work builds upon previous work by Babst et al. (2013) by examining the relationship in a

more complex system and over a longer time period. We had the benefit of using one of the longest available datasets for eddy flux in the USA (extending back to 1996) to compare with annual biomass growth (derived from tree-ring series). This long-term dataset allowed us to identify the relationship between the two methods and isolate potential lag-periods of tree growth. Biomass increments derived from tree-ring series could validate annual eddy flux summaries using simultaneous measurements of ecosystem productivity. These biomass increments could provide an alternative methodology for tracking ecosystem CO_2 gain in systems without established flux systems, providing a more cost-effective alternative to flux measurements.

1.2 Methods

1.2.1 Site Description

This study was conducted in the Howland Research Forest in central Maine, USA (Figure 1.1). The Howland Research Forest is widely recognized for its long-term research in forest ecosystem science (see Rustad 1994; Hollinger et al. 1999; Davidson et al. 2002; Richardson et al. 2009). The site was established in 1987 through a partnership between the University of Maine and International Paper. Collaborations between the US Forest Service, US Department of Energy, NASA, and the University of Maine have maintained an active research program focused on carbon and nutrient cycling. In 2007, the 220-hectare site was purchased and permanently protected by Northeast Wilderness Trust.

In total, the site maintains four eddy flux towers; two towers (the “main” and “west” towers) are located in a mature spruce–hemlock stand approximately 800 m apart (Hollinger et al. 2004). The site has the second longest running flux record in the US, dating back to 1996 (the longest belonging to Harvard Forest). These 20 years of data provide a time series long enough for robust analyses of relationships between CO_2 flux

and various environmental variables. This long-term dataset is ideal for comparisons to biomass growth.

A mature multi-aged spruce–hemlock forest comprises approximately 170 of the 220 hectares owned by Northeast Wilderness Trust (outlined in yellow in Figure 1). The forest is dominated by red spruce (*Picea rubens*) and eastern hemlock (*Tsuga canadensis*), consisting of approximately 90% conifer, and 10% deciduous tree species. A summary of the species and stand descriptors of Howland Forest is presented in Table 1.1, with additional information in Table A.1 of the Appendix. Soils are spodosols, formed in well- to poorly-drained glacial till with very little elevational change. The climate is damp and cool, with average annual temperatures of 6.2°C and a mean annual precipitation of 1148 mm (Daly et al. 2008). The site has evidence of previous logging (evenly distributed well-decayed cut stumps), but has been unmanaged for roughly a century. Compared to other stands of the region, this stand represents a highly complex system in both size and age distributions of trees. The site supports several remnant trees in excess of 300 years old, along with many standing dead trees, and pit-and-mound topography.

Table 1.1: Forest descriptors by species in the Howland Forest NASA plot (2015 inventory). Species ranked by decreasing relative density. Additional information presented in Table 1.1Table A.1 of the Appendix.

Species	Relative density	Relative basal area	QMD* (cm)
Red spruce (*Picea rubens*)	0.447	0.413	21.3
Eastern hemlock (*Tsuga canadensis*)	0.278	0.276	22.1
N. white-cedar (*Thuja occidentalis)*	0.108	0.086	19.8
Red maple (*Acer rubrum*)	0.090	0.069	19.3
White pine (*Pinus strobus*)	0.049	0.140	37.5
Balsam fir (*Abies balsamea*)	0.021	0.006	11.7
Yellow birch (*Betula alleghaniensis*)	0.004	0.007	28.5
Paper birch (*Betula papyrifera*)	0.003	0.003	20.3

*Quadratic mean diameter

A 3-ha permanent plot (150 × 200 m) whose center lies 240 m north of the main tower (Figure 1.1), was established in 1989 by the Laboratory for Terrestrial Physics at NASA's Goddard Space Flight Center for remote sensing and ecosystem dynamics research (see Weishampel et al. 1994; Ranson et al. 2001; Sun et al. 2011). At that time, all living and dead plot trees 3.0 cm diameter and larger at breast height were mapped and measured (diameter and total height), recording ca. 7,800 stems. Each tree was tagged using a unique identification number for later re-measurement. This large mapped plot is subsequently referred to as the NASA plot.

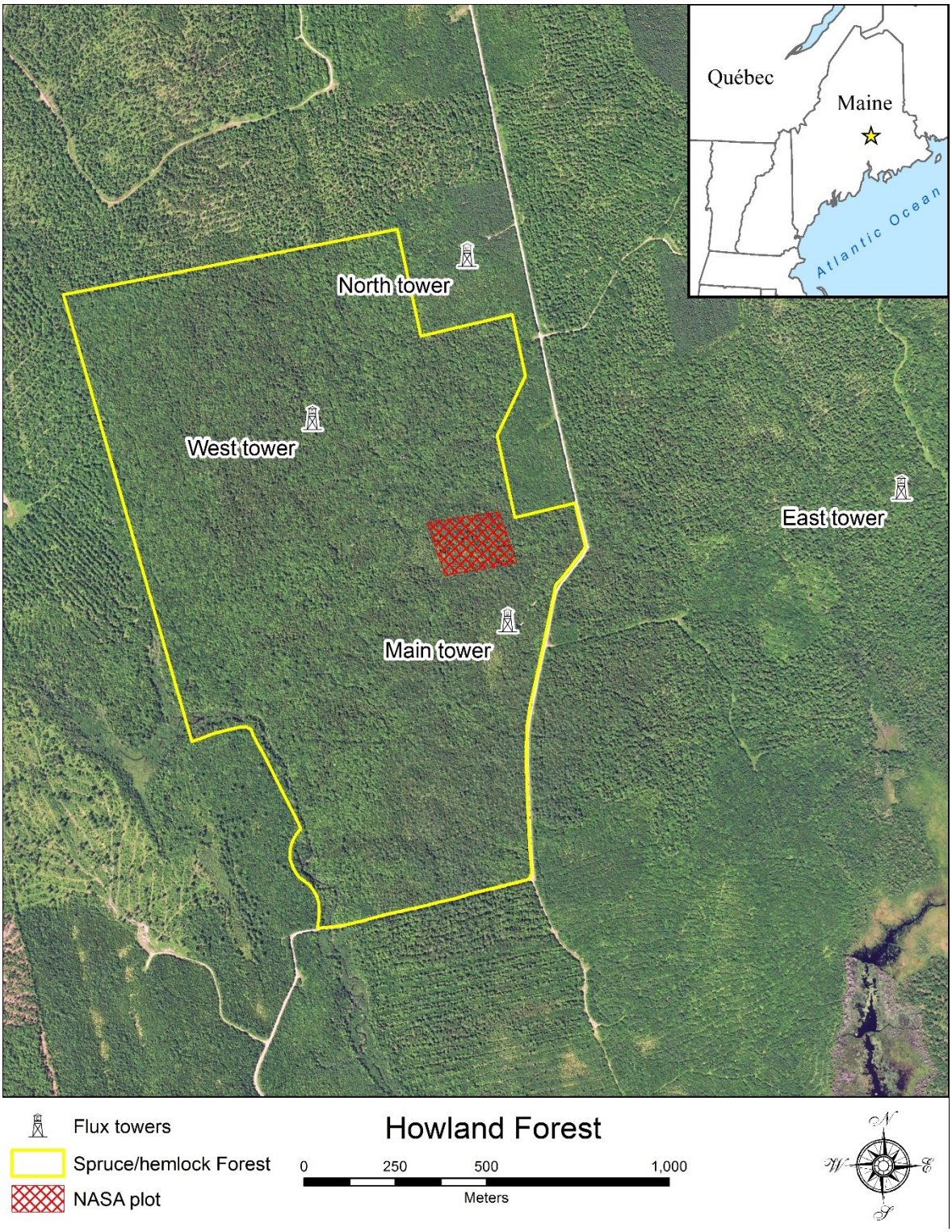

Figure 1.1: Howland Forest location map, showing the location of flux towers and the NASA plot.

1.2.2 NASA plot re-inventory

In 2015 we re-mapped and re-measured all living and dead standing trees >10 cm diameter at breast height (DBH, 1.37 m) in the NASA plot. The mapping was conducted using 5-m wide belt transects running from the southern to the northern boundary (40 belt transects of 150 m). Each tree was identified by species, measured at breast height, and given an X-Y coordinate in relation to the southwestern corner. When necessary, previous tags were repositioned on trees at breast height. Matching trees to their original tag number was a challenge throughout mapping, and care was given to identifying trees with missing tags. Trees without original tags were labeled with write-on metal tags. In the case of an ingrown tree (one that achieved the minimum diameter threshold between 1989 and 2015) or unknown tag, the tree was labeled with a new unique number.

We assessed data quality by cross-referencing all tree's original tag numbers, species, diameters, and X-Y coordinates to 1989 records. Field checks were conducted for trees with abnormal measurements (ca. 1% of trees), species (ca. 3%) and mortality (<1%) disagreements, and mismatched tag numbers. In some cases records were not available for 1989 trees (e.g., trees added along the perimeter and unknown interior trees, representing ca. 1% of trees). When the original (1989) diameters were not available, the 1989 diameters were predicted using a linear regression based on species and diameter change from all other trees from that species. Trees with equal or slightly smaller current diameters than those recorded in 1989 were assumed to have zero growth, and therefore no increase in carbon mass.

The 2015 tree dataset was georeferenced based on coordinates collected along the plot boundary with a Trimble GeoXT and external antenna. Plotting the 3-ha plot boundary, which was originally thought to be rectangular, revealed a parallelogram shape. To georeference individual trees, the raw X-Y coordinates were converted to UTM

coordinates in relation to plot-origin in the southwestern corner. The points were shifted to reflect the parallelogram shape (the north border shifted 9.86º from east to west). The entire plot was then shifted 9.79º counterclockwise to align the southern boundary on the Howland/Edinburg town line. Additional small adjustments were made to align individual trees to a LIDAR based digital surface model (aligning white pine canopies, clearly visible in the digital surface model). The parallelogram shape results in a slightly smaller area than a rectangular plot with the same dimensions. We estimate the plot to be 2.96 ha when accounting for the parallelogram shape. Because the 1989 dataset was mapped with the same X-Y coordinates as the 2015 dataset, it was also georeferenced using the same procedure.

Combined, the mapped datasets from 1989 and 2015 provide an ideal opportunity to track long-term mortality, ingrowth, diameter growth, and carbon pool change at the stand-level. These two inventories are used to estimate total tree carbon pool size in 1989 and 2015, accounting for tree mortality and ingrowth. The total carbon mass of all trees was summed and expressed on a per-area basis to estimate carbon pool size (in Mg/ha). These data are useful for studying long-term forest dynamics, but cannot be used to track annual variability in carbon mass change.

1.2.3 Carbon mass increment

Annual carbon mass increment was estimated from increment cores collected from a 10% subset of trees on the NASA plot at the end of the growing season in 2015. The subset was selected in a random stratified (by species and diameter class, using 10-20, 20-30, >30 cm classes) manner, resulting in 327 trees. Although no spatial constraints were placed on the selection process, the large number of trees selected ensured adequate spatial distribution throughout the plot (visually assessed; see Figure 1.4). The random subset is assumed to represent all living trees >10 cm DBH in the plot, ranging

from understory suppressed trees to overstory dominants. The height, height to crown base, and canopy class were recorded for the subset. One core was extracted from each tree at breast height with a standard 5.2 mm increment borer (Häglof Company Group, Långsele, Sweden). Cores were transported to the dendrochronology laboratory at the University of Maine where they were air-dried and secured to wooden mounts. Cores were sanded and polished using increasingly fine sandpaper. Ring-widths were measured to the nearest 0.01 mm using a Velmex sliding stage (Velmex Inc., Bloomfield, NY, USA) with MeasureJ2X software (VoorTech Consulting, Holderness, NH, USA) and stereomicroscope. Cross-dating was performed using marker years, usually light or narrow rings, followed by statistical cross-dating using COFECHA software (Holmes 1983). Numerous missing rings were identified and corrected in understory red spruce and eastern hemlock.

Tree ring measurements were used to back-calculate historical diameters for every year since NASA plot establishment in 1989. Species-specific bark factors (Dixon and Keyser 2011) were used to estimate inside bark diameters in 2015. When possible, ring-widths were adjusted so that cumulative ring width equaled half the inside bark diameter in 2015, following justification presented by Frelich (2002). This adjustment compensates for off-center piths, but is only possible if cores include or approach the pith (<15 mm) and are not affected by central rot. Ring-widths were sequentially subtracted from 2015 inside bark diameter to estimate each year's diameter inside bark. Predicted bark thickness was then added back to each year's inside bark diameters for use in allometric equations. Heights were also back-calculated using heights measured in 1989 and 2015. Annual height growth was assumed to reflect ring-width growth and was calculated by multiplying the total height growth by the ratio of ring-width to cumulative radial growth since 1989, similar to methods presented by Kariuki (2002).

Tree bole mass was estimated for each tree and each year from 1989 to 2015 using three species-specific allometric equations: Honer, Taper, and Young (Honer 1967; Li et al. 2011; Young et al. 1989). Updated Honer equations from Li et al. (2011) were used for all conifer species, but original Honer equations, which have not been updated, were needed for hardwoods (representing less than 10% of trees). Taper equations were also from Li et al. (2011). The Honer and Taper equations use height and outside bark diameter to estimate inside-bark and outside-bark volume of the main stem. Corresponding heights and diameters for each year were used to estimate bole volumes with and without bark. The difference between predicted inside and outside bark volumes was used to estimate bark volume. Volumes were multiplied by species-specific wood and bark specific gravities (Miles and Smith 2009) to produce mass estimates.

The advantage of using Young's equations for carbon accounting is the ability to estimate whole tree dry mass directly, without the need to convert bole volume to mass, as required by the Honer and Taper equations (above). Further, Young's equations can produce dry mass estimates for the bole, branches, leaves, and coarse roots individually or as a whole. However, Young's equations are considered less accurate because, unlike the Honer and Taper equations, they only use diameter outside-bark and do not require tree height. We compared mass estimates from Young's stem-only equations to those produced by the Honer and Taper equations to test its applicability for our data.

The dry mass estimates produced from the allometric equations were converted to carbon mass by multiplying by species-specific carbon ratios (Lamlom and Savidge 2003). Carbon mass was summed for the cored trees, and the resulting time series reflects the year-to-year variability in carbon mass. However, to express carbon mass increment on a per-hectare basis, we needed to extrapolate growth from sampled trees to that of the entire NASA plot.

Ring-width data from cored trees was used to estimate annual growth of the non-cored trees, using a linear mixed-effects model. The fixed effects included 1989 diameter, radial growth since 1989, tree elevation (extracted from digital elevation model), and canopy class. The random effects were year nested within species, producing different intercepts for each combination. The annual ring widths thus predicted were then adjusted to match the cumulative field-measured growth from the two sampling periods. Diameters outside bark for all years were estimated using the same procedure as for cored trees. Despite using all available data to improve these ring-width models, annual productivity estimates from this modeling approach were distorted and problematic.

As an alternative approach, we scaled our cored-tree data to the plot-level based on the assumption that the randomly-selected cored trees adequately represent the entire tree population on the NASA plot. To this end, we estimated percent annual radial growth for each species across the same diameter classes used for stratification (i.e., 10-20, 20-30, >30 cm). This approach assumes trees within the same species and diameter classes are growing similarly, which we believe is reasonable, given the relatively large number of cored trees (N=327) and the stratified random selection we employed to select them.

The annual biomass increment was thus calculated for every tree in the 2015 inventory period based on predicted ring-widths using the latter method described above. Trees that died over the study period were not included because of unknown mortality dates. Trees that died were generally small-diameter (Table A.1 in the Appendix), presumably slow-growing suppressed trees, and thus contributed little to carbon mass increment.

1.2.4 Annual carbon flux

CO_2 flux was measured at a tower height of 29 m and summarized from 1 January 1996 to 31 December 2015 as 30 minute averages in units of micromoles CO2 m^{-2} s^{-1}. The flux system on the main tower consisted of a SAT-211/3K 3-axis sonic anemometer (Applied Technologies, Inc., Boulder, CO) and model LI-6262 fast response CO_2/H_2O infrared gas analyzer (LiCor Inc., Lincoln, NB). Air was ducted from the tower through 50 m of 3.2 mm high-density polyethylene tubing, regulated by mass flow controllers at a rate of 4 L /min. The model LI-6262 analyzer was replaced with a LiCor model LI-7200 closed path analyzer in 2012. Tube length and flow rate remained unchanged. Detailed Howland flux procedures, including gap-filling and quality control can be found in Hollinger et al. (1999, 2004). Data were converted to grams of carbon per square meter and summarized by day.

The annual carbon flux was first summarized for each year since 1996 as the cumulative net ecosystem exchange (g C m^{-2} yr^{-1}). Tower based estimates of net carbon flux are typically reported in negative units, as they reflect a micrometeorological sign convention where flux from the atmosphere is negative. For comparison to biomass increment in trees, we report carbon flux from the forest pool perspective; carbon into the forest is accumulated to positive values, while carbon loss to the atmosphere is negative (as presented in Richardson et al. 2013).

1.2.5 Linking carbon mass increment and annual carbon flux

Yearly summaries of CO_2 flux are typically summarized by calendar year. Calendar year summaries are practical for carbon accounting purposes or comparisons between sites, but this timeframe holds little biological significance. Several studies have avoided a mid-winter (calendar year) split by beginning the flux year in the previous year's autumn

(Goulden et al. 1996; Pereira et al. 2007). Thomas et al. (2009) summarized carbon fluxes by hyrdo-ecological year to study flux response to drought. Here we adopt a similar approach for summarizing flux; however, we target the date at which stem growth terminates (i.e., end of growing season before leaf senescence). By incrementally shifting the date used to separate flux years and comparing the correlation between carbon mass increment and carbon flux at each shift, we determined the optimal shift for comparing the two metrics for these data. In theory, this should roughly correspond with the date trees stop allocating carbon to growth.

1.3 Results

1.3.1 NASA plot re-inventory

Locations of geo-referenced trees for the initial 1989 and current 2015 sampling periods are presented in Figure 1.2 and Figure 1.3, emphasizing the parallelogram plot shape. The points, representing individual trees, are overlaid on a LIDAR-derived digital canopy surface model, with lighter colors representing taller vegetation. Dark areas represent canopy gaps and generally align with the gaps in the mapped tree distribution. The tallest canopy heights captured from LIDAR align with mapped white pines, which are the tallest canopy trees in the NASA plot. The subset of trees randomly selected from the 2015 inventory for coring is shown in Figure 1.4.

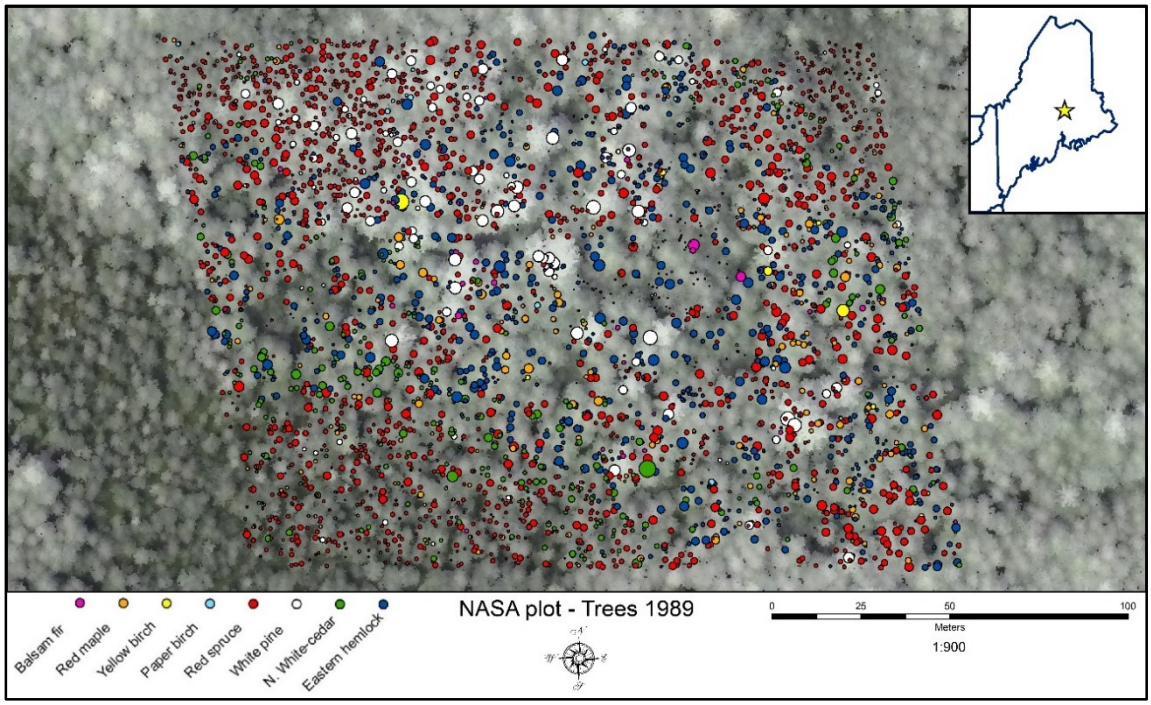

Figure 1.2: Locations for all NASA plot trees greater than 10 cm DBH in the initial 1989 inventory. Point size is relative to tree diameter. The points are plotted over a LIDAR-derived digital canopy surface model from 2015.

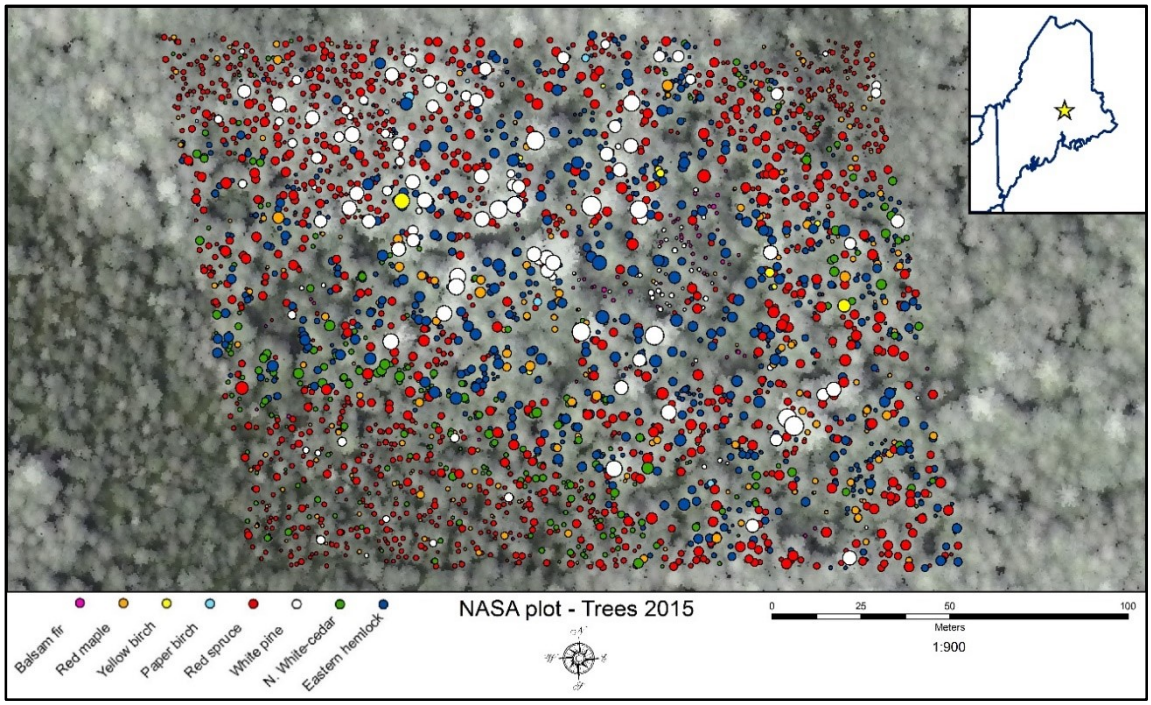

Figure 1.3: Locations for all NASA plot trees greater than 10 cm DBH in the initial 2015 inventory. Point size is relative to tree diameter. The points are plotted over a LIDAR-derived digital canopy surface model from 2015.

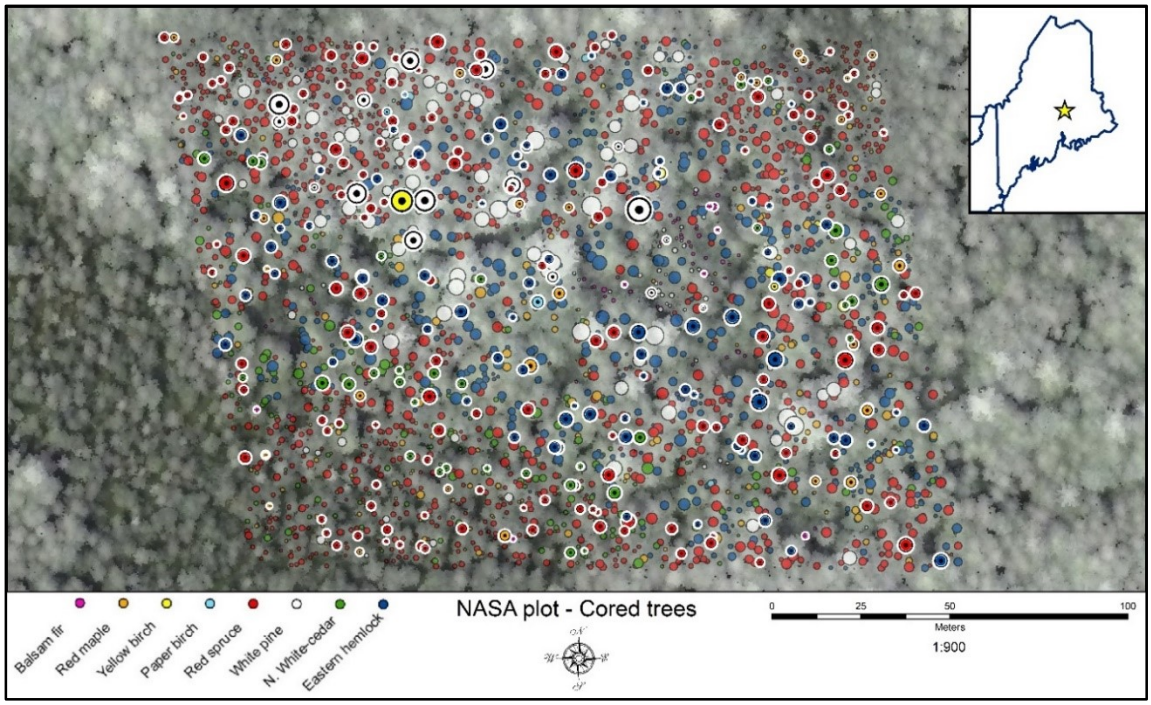

Figure 1.4: Locations for all NASA plot trees selected for coring (2015) are shown with white border and black center. These trees represent a 10% stratified random selection by diameter class and species.

The size of the living tree carbon pool was estimated for both 1989 and 2015 (Table 1.2 outlines the carbon storage change for all trees, and changes in species-level carbon storage are presented in Table A.2 in the Appendix). Specifically, tree growth, mortality and ingrowth (small trees that achieved 10 cm DBH between 1989 and 2015) were assessed to determine how the living carbon pool changed over the time period. Ingrowth (541 trees) exceeded tree mortality (507 trees) in the plot. Trees in the 1989 dataset experienced 16.4% mortality over the 26-year period, or 0.6% per year, predominantly in the smaller diameter classes. Metrics for living trees and trees that died between the sampling period are presented in Table A.1 of the Appendix.

Table 1.2: Forest descriptors for all trees in NASA plot at establishment (1989) and re-measurement (2015). Stem and whole-tree carbon mass were calculated using equations presented by Young et al. (1989).

Forest descriptors	Inventory 1989	Inventory 2015
Trees per hectare ≥10 cm	1,044	1,055
Basal area (m^2 / ha)	29.4	40.6
Quadratic mean diameter (cm)	19.0	22.1
Stem carbon mass (Mg / ha)	42.2	63.8
Total tree carbon mass (Mg / ha)	72.8	108.0

1.3.2 Carbon mass increment

Stem mass estimates from the three allometric equations (Honer, Taper, and Young) through time were very closely related, yet differed as much as ca. 15% in magnitude (Figure 1.5). The Young equation produced stem carbon mass increments ca. 5% greater than the Honer equation and ca. 10% less than the taper equation. This close relationship between the Young equation and the two height-based equations validates the use of Young's equations for our study, despite the fact that it does not include tree height as a predictor. We thus estimated the total carbon mass increment from trees using Young's complete tree equation (including stem, branches, leaves, and coarse roots).

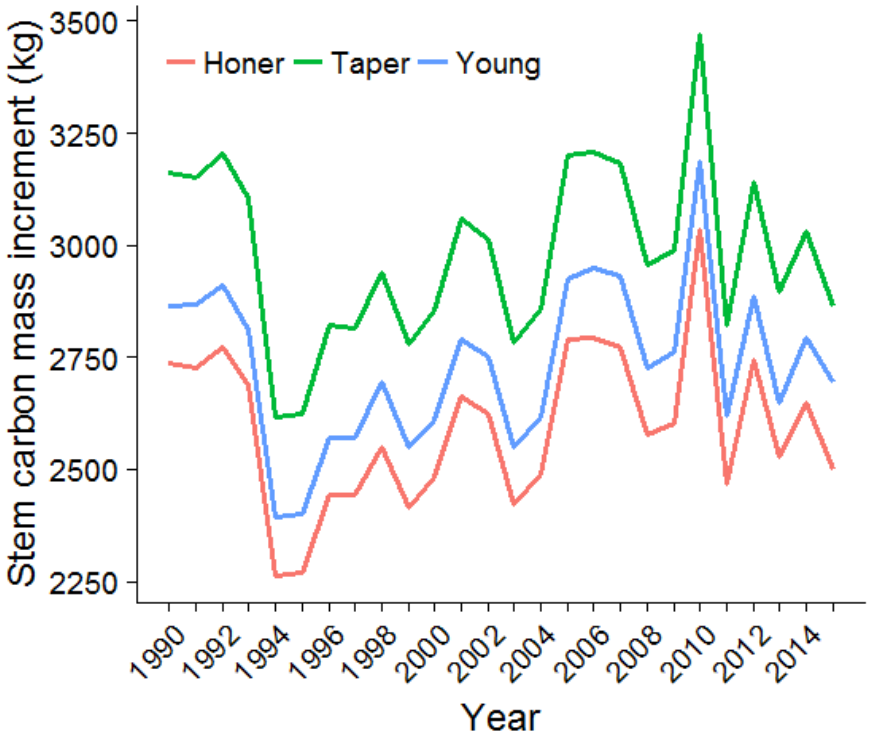

Figure 1.5. Total stem carbon mass increment of 327 cored trees using the three allometric stem volume equations: Honer, Taper, and Young.

The total plot-level annual carbon mass increment (scaled to the entire plot, using growth data from the subset of cored trees) showed marked fluctuations over the sampling period, ranging from 131.1 to 176.9 g C / m^2 (Figure 1.6). The lowest carbon mass increments over this timeframe were in years 1994 and 1995, immediately preceding the flux tower establishment. The most productive year in terms of carbon mass was 2010.

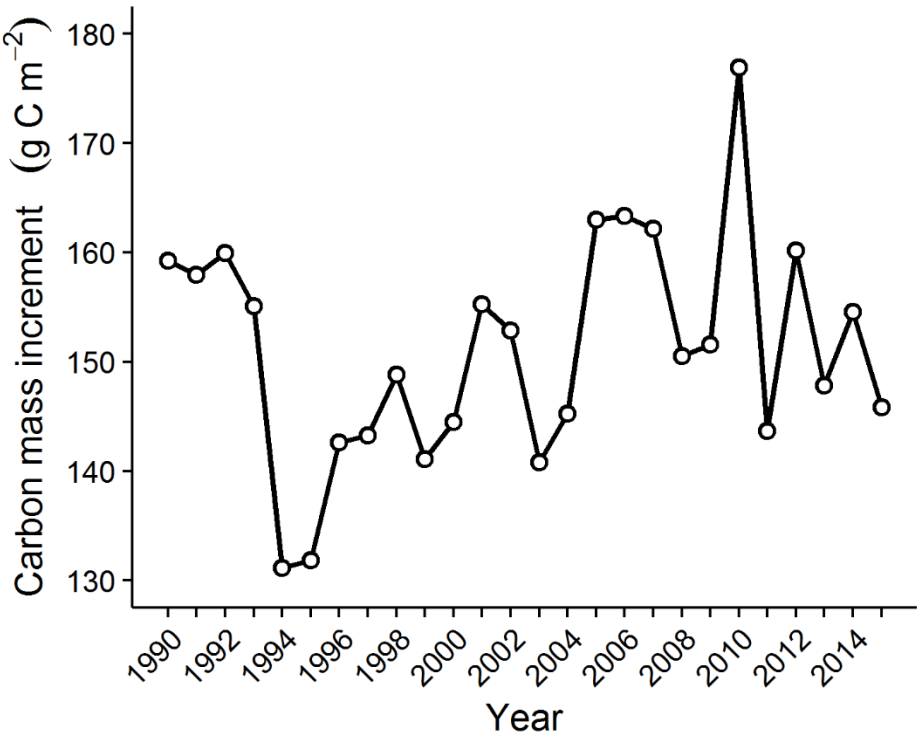

Figure 1.6: Annual carbon mass increment predicted for the 3-ha NASA plot based on all trees ≥10cm.

1.3.4 Annual carbon flux

By incrementally shifting the dates used to define annual CO_2 flux summaries, we determined the period with the strongest correlation with carbon mass increment. To illustrate the influence of shifting the start period for defining a flux year, the un-shifted calendar year flux is presented alongside one of the shifted time series representing annual flux summarized from previous year's 1 September to the following 31 August (Figure 1.7).

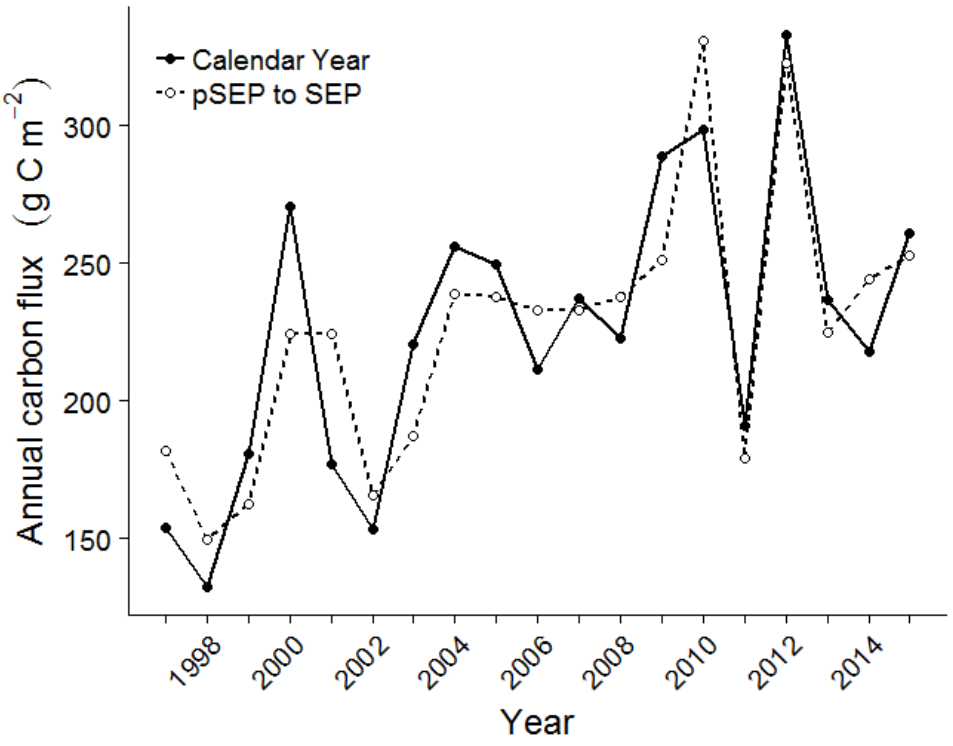

Figure 1.7: Comparison between two annual flux summaries that differ with respect to how a CO_2 flux year is defined. The solid line represents the standard approach (calendar year), and the dashed line represents a summary from previous September (pSEP) to current September (SEP).

1.3.5 Linking carbon mass increment and annual carbon flux

Carbon mass increment series derived from increment cores was not well correlated with the annual carbon flux time series based on calendar year (r = 0.43). However, as the yearly flux summary was shifted (as above), the correlation improved dramatically (Figure 1.8). For example, we found that the correlation could be maximized (achieving a correlation of r=0.72) by defining a flux year as 23 August of the previous year to 22 August of the following year. Based on this result, and constrained by the need to later use monthly climate data to explore climate-growth relationships (Chapter II), we chose to summarize the annual carbon flux data from previous 1 September to the

following 31 August (r = 0.70), allowing us to better assess the year-to-year relationships with carbon mass increment (Figure 1.8).

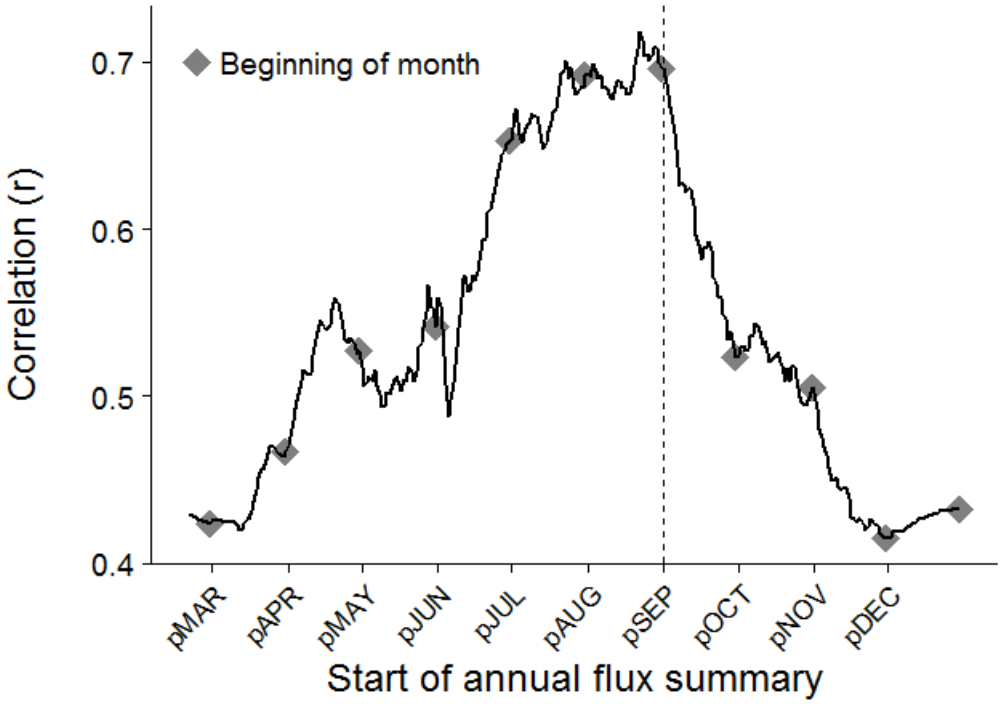

Figure 1.8: The correlation with carbon mass increment when annual flux starting dates are incrementally shifted into the previous year. The solid line represents correlation when incrementally shifted by day, and diamonds are correlation when shifted by month. The vertical dashed line illustrates the highest monthly correlation at 1 September (r=0.70). The prefix *p* refers to previous year.

The mean annual carbon mass increment (derived from tree-ring series) since 1996 was 152.1 ± 9.5 g C / m^2 compared to 223.9 ± 49.0 g C / m^2 of annual carbon flux based on eddy flux measurements. When plotted together on respective scales (Figure 1.9), carbon mass increment and annual carbon flux demonstrate a strong visual association. However, the relationship is interrupted by a striking shift that occurred ca. 2007. Prior to that shift, the carbon mass increment shows a distinct one year lag behind the annual carbon flux data (Figure 1.9), a pattern also recognized by Richardson et al. (2013). However, after ca. 2007, this relationship changes, with flux and carbon mass

increment becoming more synchronous. Comparisons between species-level carbon mass increment and annual carbon flux are presented in Figure A.1 of the Appendix.

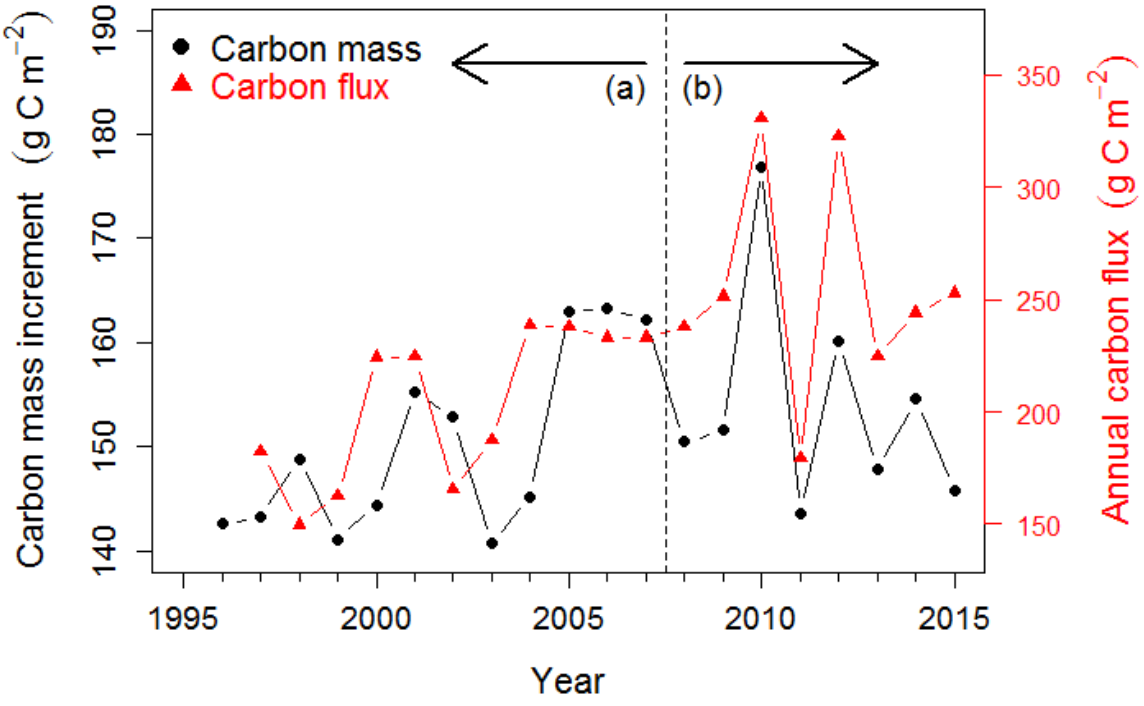

Figure 1.9: Comparison of carbon mass increment (derived from tree-ring series) and shifted annual carbon flux (eddy flux data) from previous year September to following September. The vertical dashed line represents a split into two time periods, time series (a) and time series (b), representing a shift from a one-year lag to synchrony in the series.

By separating carbon mass increment in two segments (time series (a) = years 1996-2007; time series (b) = years 2008-2015, Figure 1.9) we can determine the optimal annual flux period for each time series using the same shifting procedure as that presented in Figure 1.8. Shifting the annual flux period 16 months before growth begins (the September from two years prior) yields a year-to-year correlation as high as 0.95 for time series (a) (Figure 1.10). In contrast, if we shift time series (b) to the same period 16 months before, the correlation shows a negative correlation (r=-0.47). Alternatively, shifting the flux period back just 4 months for time series (b) to the previous September results in

another strong positive correlation (r=0.86). Data corresponding to wood formation in 1996 and 1997 are unavailable if flux summaries are shifted 16 months.

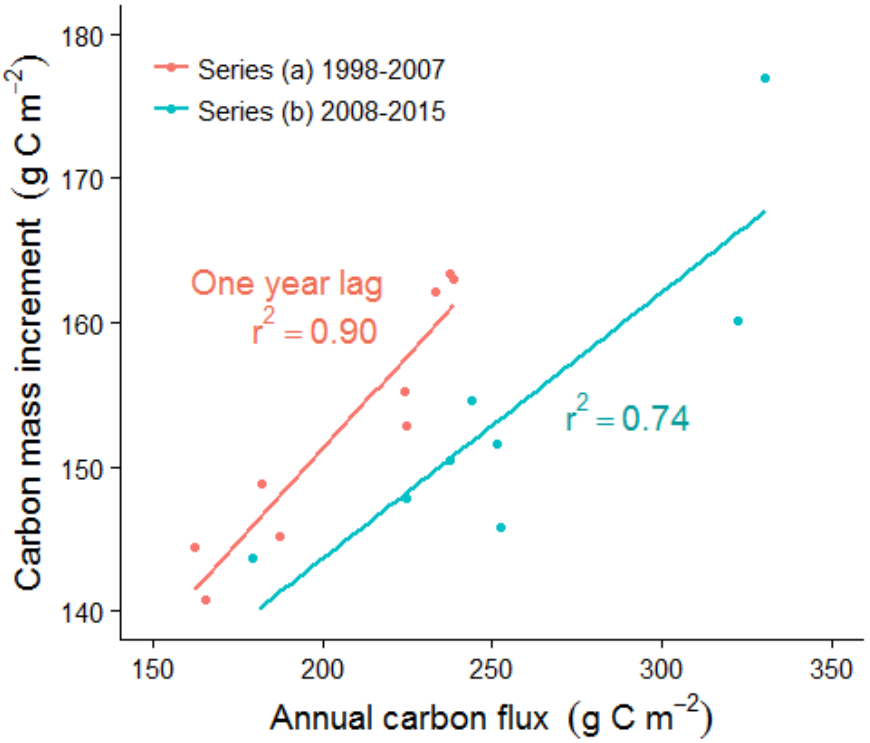

Figure 1.10: Correlation between carbon mass increment (derived from tree-ring series) and annual carbon flux (eddy flux data). The series are separated based on years of wood formation. Both flux summaries begin on 1 September, but correlations with series *a* (1998-2007) used flux summaries starting two Septembers before wood formation, while *b* (2008-2015) used flux starting the previous year's September.

1.4 Discussion

1.4.1 Linking carbon mass increment and annual carbon flux

We demonstrated that shifting the dates used to demarcate annual carbon flux summaries clarified the link between carbon mass increment and annual carbon flux. Using incremental daily shifts, we determined the optimal shift period for carbon flux data based on 20 years of tree growth. We chose to summarize flux from the previous year's 1 September to 31 August because this monthly cut-off showed the highest correlation with

carbon mass increment (optimal day cut-off is 23 August). Starting the flux summary in September corresponds with the cessation of radial growth and the end of latewood formation of cool-weather conifers of North America (Deslauriers et al. 2003; Thibeault-Martel et al. 2008; Duchesne et al. 2012) and thus provides strong biological justification for this shift. That is, the shifted dates better represent the time period in which carbon flux is being allocated to a given year's tree growth. This shift allowed us to identify the one-year lag in growth and could similarly clarify relationships at other flux sites.

When plotted together, the first portion of the study period shows carbon mass increment with a clear one-year lagged time series behind annual carbon flux, followed by a dramatic shift to synchrony occurring ca. 2007 (Figure 1.9). We interpret the early lag period as evidence that a large portion of carbon assimilated by photosynthesis was not allocated to structural growth until one year later, a finding also reported by Richardson et al. (2013) from this same site. Specifically, the magnitude of the previous year's flux reflected the amount of available storage that could be allocated to growth the following year. It is unclear if the lag was in response to some change in tree physiology, such as stress or reproductive effort. In unfavorable conditions (e.g., drought), stressed trees can allocate more carbohydrates to storage than to growth, maintaining reserves to improve chances of survival (Hartmann and Trumbore 2016).

We suspect the shift to synchrony between carbon mass increments and the annual carbon flux measurements that took place ca. 2007 (Figure 1.9) reflects the onset of favorable early season conditions. During such conditions, current photosynthate could be immediately allocated to growth once translocated (Kozolowski 1992). This synchrony is emphasized by peaks of both measurements in years 2010 and 2012, both of which had early snow melt (unpublished site data) and above-average spring temperatures (Figure 2.9 in the following Chapter). These two productive years were interrupted by a

below-average year in 2011. Favorable spring conditions can cause an earlier onset of photosynthesis leading to increased annual productivity (Black et al. 2000; Hollinger et al. 2004; Richardson et al. 2009). Wood formation is known to rely on a combination of new and old assimilates (Keel et al. 2006), but these ratios depend on a number of environmental factors. We suspect years with favorable early season conditions would have a higher ratio of new carbon than stored carbon being allocated to stem growth. In contrast, favorable late-season conditions would result in higher allocation to storage given that stem xylem tissue is not actively being produced at this time (Kuptz et al. 2011).

On average, annual carbon flux at this site is a net sink until 7 November (day-of-year 310) (Figure 1.11). Because radial growth ceases in August or early September in this region (Deslauriers et al. 2003), photosynthate produced from September through early November cannot be allocated to stem growth until the following season. We suspect the majority of this late season photosynthate is allocated to storage (Kuptz et al. 2011) with lesser resources allocated to other plant functions such as cell wall thickening of latewood (Babst et al. 2013; Cuny et al. 2015), fine root development (Hendrick and Pregitzer 1993), or maintenance respiration (Ryan et al. 1997). In temperate and boreal regions, stored carbohydrates allow trees to begin structural growth as soon as conditions are suitable the following year (Barford et al. 2001; Gough et al. 2009). Carbohydrate storage also has important physiological functions within a tree, aiding in osmoregulation and increasing cold-weather hardiness (Hartmann and Trumbore 2016). Both conifer and hardwood species accumulate non-structural carbohydrates over the growing season; Dietz et al. (2014) speculate that trees reach their annual storage maximum just before the dormant season.

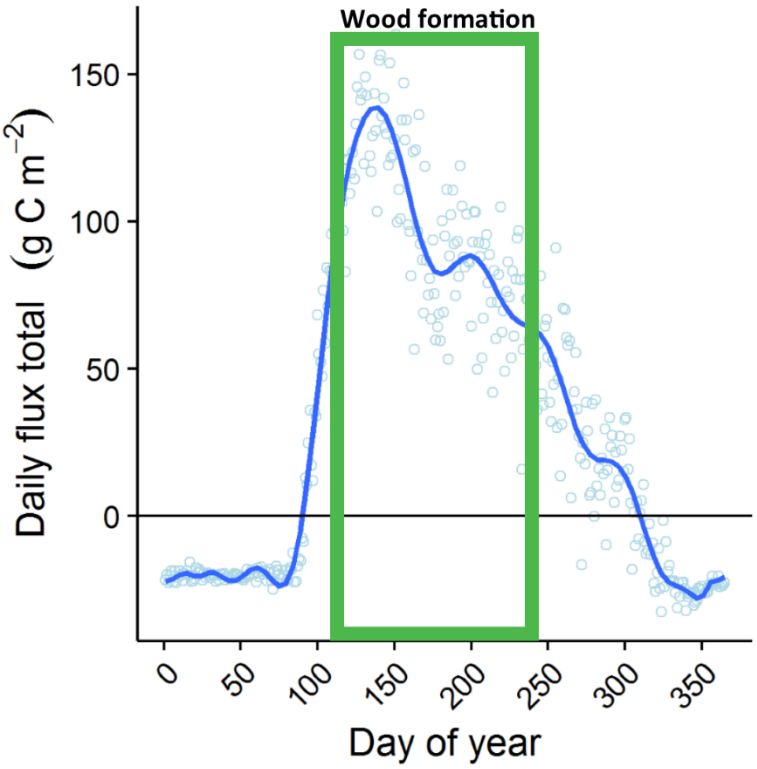

Figure 1.11: Representative annual time series of daily CO_2 flux (blue circles) based on medians from 1996-2015 with smoothing spline. The green box represents the estimated season of wood formation based on data from Duchesne et al. 2012 (extended in spring).

Of course tree growth is not entirely limited by carbon supplied from stored non-structural carbohydrates (Körner 2003); limitations on growth also result from environmental or developmental factors. Wood formation is more temporally restricted than is photosynthesis on an annual basis. Some trees may allocate 80% of a year's growth from the end of May to mid-July (Deslauriers et al. 2003), reaching maximum growth rates with maximum day length (Rossi et al 2006; Duchesne et al. 2012). At Howland Forest, trees are fixing carbon for ca. 210 days on average based on flux tower data (Figure 1.11); however, radial growth is restricted to a much shorter time period. For example in the boreal forest of Quebec, albeit a cooler climate, the wood formation (i.e. from start of radial growth to end of cell wall thickening) was restricted to an average season length of 93 days from 2004-2010 (Duchesne et al. 2012). We likewise suspect

that wood formation at Howland Forest is restricted to smaller time frame than is photosynthesis. Because trees in cold climates are restricted by growing season length (Körner 2003), it may be beneficial to store carbohydrates until conditions are favorable in the following year (Hartmann and Trumbore 2016).

We did not expect to find the shifts in annual carbon allocation strategies described above. Although individuals shift allocation patterns through development, and species are known to have distinct allocation patterns, (Kozolowski 1992), a shift in stand-level carbohydrate strategies is a novel finding to the best of our knowledge.

1.4.2 Carbon pool change

Re-measuring the NASA plot, accounting for mortality and ingrowth, revealed a large increase in forest carbon mass since plot establishment in 1989. The number of trees (>10 cm), the quadratic mean diameter, and total biomass each increased from 1989 to 2015. The mortality rate (0.6% per year) falls below published values for old-growth forests of the region (Fraver et al. 2009; Lorimer et al. 2001), and the number of trees that died was exceeded slightly by the number of ingrowth to the 10 cm diameter class. The carbon stored in living trees increased by 48% over the 26-year sampling period. Carbon dynamics of old forests are thought to reach a theoretical plateau in living carbon storage (stored in living trees and deadwood) (Bormann and Likens 1979; Law et al. 2003). Howland Forest does not appear to be near a plateau in carbon storage, indicated by the rapid accumulation of carbon mass in living trees. Without disturbance, we expect the carbon stocks will continue to increase through development, as has been shown in other studies of mature forests worldwide (D'Amato et al. 2011; Luyssaert et al. 2008; Pregitzer and Euskirchen 2004).

1.4.3 Implications for future studies

Although our data show strong correlations between the two metrics of productivity, our methodology yielded carbon mass increment that accounted for only 68% of the total annual carbon flux measurements over the sampling period. This discrepancy is likely a combination of conservative carbon estimation from trees (i.e. allometric equations do not account for fine root and litter production) and perhaps to carbon sequestered by saplings and understory vegetation. Fine root productivity may account for 200 - 300 g / m^2 of dry mass (Cronan 2003; Finér et al. 2011), while litter production contributes another 230 - 400 g / m^2 (unpublished site data). These two pools alone can account for the discrepancy between carbon mass increment and annual carbon flux if we assume 50% carbon content in dry mass. One study accounted for 99% of carbon flux over a five-year period by accounting for all carbon pools, including fine and coarse roots, detrital inputs from woody debris and leaf-litter, and herbivory (Gough et al. 2009). It is unclear how these un-tallied carbon pools would affect the annual variability of carbon mass increment in our study, and whether they could further clarify the relationship with annual carbon flux.

This finding stimulates a number of new and exciting questions. Can we demonstrate that a shift in allocation strategies is triggered by environmental cues? Do stands in temperate and boreal climates typically change allocation strategies several times in one tree's lifespan? Can a lag in growth be an indication of stand-level stress? More research is needed to address these questions.

1.5 Conclusions

This project attempted to characterize the year-to-year relationship between carbon mass increment and annual carbon flux. Our results demonstrate compelling

evidence that a relationship exists between the two metrics of forest productivity, and that the carbon mass estimated from tree-rings can be traced to CO_2 flux measurements from towers. However, year-to-year allocation strategies are subject to change based on physiological conditions of the trees. To the best of our knowledge, the trade-off between storage and growth allocation has never been illustrated at the stand-level. Our results suggest year-to-year changes in stand-level carbon allocation strategies. Allocation strategies may not remain constant through time because photosynthesis and wood formation are constrained by a different set of environmental conditions (Rossi et al. 2006; Körner 2015). Under periods of stress, trees may refrain from allocating non-structural carbohydrates to stem growth (i.e. storage) until the return of more favorable conditions (Klein et al. 2014). Non-structural carbon storage is most likely responsible for the discrepancies seen between CO_2 flux and tree biomass increment from tree-rings (Babst et al. 2013; Gough et al. 2009), causing lags between CO_2 flux and tree growth. The twenty-year record at Howland allowed us to observe a shift in usage of these stores.

Our results suggest that the two metrics of forest productivity are measuring different tree responses to their environment. Carbon mass increment reflects the conditions for wood formation and available storage, while annual carbon flux is an indication of total ecosystem carbon storage change, both following different annual cycles. One is often an indication of the other, but not necessarily in the same year. Under this line of reasoning, we would suspect that the previous year's climate affects the amount of stored carbohydrate available for growth, and the current year's conditions affect the extent of wood formation. This reasoning could in part explain the correlation between radial growth and previous year's climate variables often reported in tree-ring studies (e.g., Fritts 1976). Climate clearly influences both metrics of forest productivity used in our study, but it is unclear if environmental cues triggered the switch in allocation strategies

witnessed here. Additional studies on within-year growth, using electronic dendrometers, could help differentiate conditions that most strongly favor one productivity metric over the other.

In summary, we believe tree-ring derived carbon mass increment can be used as coarse proxy for long-term CO_2 flux inferences, but should be interpreted with caution. This method is comparatively fast and less expensive, and provides valuable information on climate effects on wood formation. But when used to estimate annual carbon flux, one needs to consider the variability of allocation strategies within tree species and size classes.

CHAPTER 2 : TREE, SPECIES, AND FOREST-LEVEL GROWTH RESPONSE TO CLIMATE

2.1 Introduction

Forests are the largest carbon sinks in the terrestrial biosphere, and they provide ecological services by mitigating increasing atmospheric CO_2 concentrations. However, a changing climate could affect forest productivity (Boisvenue and Running 2006) and species distributions (Iverson and Prasad 1998), potentially resulting in large annual changes in carbon sequestration. We currently have a limited understanding of forest productivity response to climate, particularly how stands (or species within complex stands) respond to changing climate. The impacts of climate change may alter the way we manage forested systems, particularly decisions made on species composition and/or age structure (Millar et al. 2007). In addition, models projecting future forest productivity sometimes misrepresent plant physiological response to climate (Richardson et al. 2012) and would therefore benefit from alternative perspectives of climate–growth relationships, particularly regarding multiple levels of organization (e.g., individual tree-, species- and forest-level).

Climate–growth relationships in forest systems are dynamic and difficult to predict because of the large variability between trees. This complexity is due in part to independent tree species responses to climate (Drobyshev et al. 2013; Friedrichs et al. 2009; Kipfmueller et al. 2010). Additionally, individuals within the same species can respond differently to climate depending on size (Mérian and Lebourgeois 2011), competition (Sánchez-Salguero et al. 2015), canopy position (Martin-Benito et al. 2008), and landscape position (Gewehr et al. 2014). Variations in soil drainage, stand density, and stand developmental stage can all affect resource (i.e. water, nutrient, and light) availability, therefore landscape and canopy positions regulate specific needs for

individual forest trees. Although climate is just one of many environmental factors affecting productivity (see Foster et al. 2016), it is often analyzed independently of these potentially confounding factors.

Much of the previous work on climate–growth relationships has relied on dendrochronology (i.e. the study of annual tree rings) because such data provide long-term replicated information with annual resolution. Tree-ring series are routinely standardized for dendrochronology studies, a process whereby long-term size- or age-related growth trends are removed from individual tree-ring series, resulting in a dimensionless index of annual growth (Cook 1987). These standardized chronologies are then combined (within a species) to produce a single species-specific chronology (e.g. Biondi and Qeadan 2008). The resulting chronology is used to investigate trends with climate variables using as many years as possible, and employing a variety of statistical analyses.

Recent work has proposed an alternative to the traditional tree-ring analyses, namely the use of annual volume or biomass increments (also derived from tree-ring series; Bouriaud et al. 2005; Lara et al. 2013; Foster et al. 2014), which may provide a more holistic picture of forest growth, in part because it produces time series in standard units used by ecosystems ecologists. Further, carbon mass increments summed by species or by area (e.g., Mg / ha) conveniently account for tree size-related trends in ring widths without the need for standardization (Foster et al. 2016). That is, summing annual carbon mass increments from trees within a stand inherently weights trees based on their rate of mass accumulation: trees sequestering more carbon are thus more influential on stand-level growth. Stand-, or species-level carbon mass increment, in comparison to standardized chronologies, may be equally informative for assessing climate effects on

forests (see Foster et al. 2016). However, analyzing climatic effects on carbon mass increment using conventional dendrochronology analyses is an un-tested concept.

Another standard procedure used by dendrochronologists involves sampling relatively large, presumably old trees that are limited by a particular resource of interest (e.g. water stress in an arid environment). The individuals are often non-randomly selected in environments that support fewer trees to avoid the confounding factors of tree-tree competition. These sampling strategies are designed to maximize the climate signal of interest, and by doing so they have provided invaluable insights into past climate variability (Lara and Villalba 1993; Sheppard et al. 2002). While these techniques may be suitable for climate reconstructions, they likely do not capture the range of growth patterns of trees growing in typical forest systems (Carrer 2011, Foster et al. 2016). Assessing climate–growth relationships for forest systems, particularly complex systems of multi-aged and mixed-species composition, requires a different methodology from that of conventional dendrochronology studies.

The objective of this study was to explore an alternative tree-ring approach for climate–growth relationships intended for complex forest systems. This work was conducted at the Howland Research Forest, a multi-aged spruce–hemlock (*Picea rubens*–T*suga canadensis*) forest of central Maine, USA. Our methodology differs in that 1) sample trees were stratified-randomly chosen to represent stand variability; 2) forest growth was estimated by summing carbon mass increments across the random selection, thereby producing species- and stand-level growth metrics. This methodology benefits from a relatively flexible unit of measure (i.e. annual carbon increment), which may be calculated at different levels of organization (e.g. tree-, species- and stand-level). Viewing forest growth at these various levels provides information on the dynamic nature of climate–growth relationships, and it provides insights into the methods we use to analyze them.

2.2 Methods

2.2.1 Site description

Our study site, Howland Forest of central Maine, USA, is widely recognized for its long-term research in forest ecosystem science (see Rustad 1994; Hollinger et al. 1999; Davidson et al. 2002; Richardson et al. 2009). The site supports 170 hectares of mature mixed-aged spruce/hemlock forest, consisting of roughly 90% conifer, and 10% deciduous tree species (Hollinger et al. 1999). The most abundant species are red spruce (*Picea rubens*), eastern hemlock (*Tsuga canadensis*), northern white-cedar (*Thuja occidentalis)*, white pine (*Pinus strobus*), and red maple (*Acer rubrum*).

Howland is located in the transition zone between the eastern deciduous forest and the boreal forest in eastern North America (Seymour and Hunter 1992). The climate is damp and cool, with average annual temperatures of 6.2°C and a mean precipitation of 1148 mm/year which is evenly distributed throughout the year (Figure 2.1). Soils are spodosols, formed in well- to poorly-drained glacial till with little change in elevation. The site has evidence of previous logging (evenly distributed well-decayed cut stumps), but has been unmanaged for roughly a century. Compared to other stands of the region, this stand represents a highly complex system in both size and age distributions of trees. The site supports several remnant trees in excess of 300 years old, along with many standing dead trees, and pit-and-mound topography.

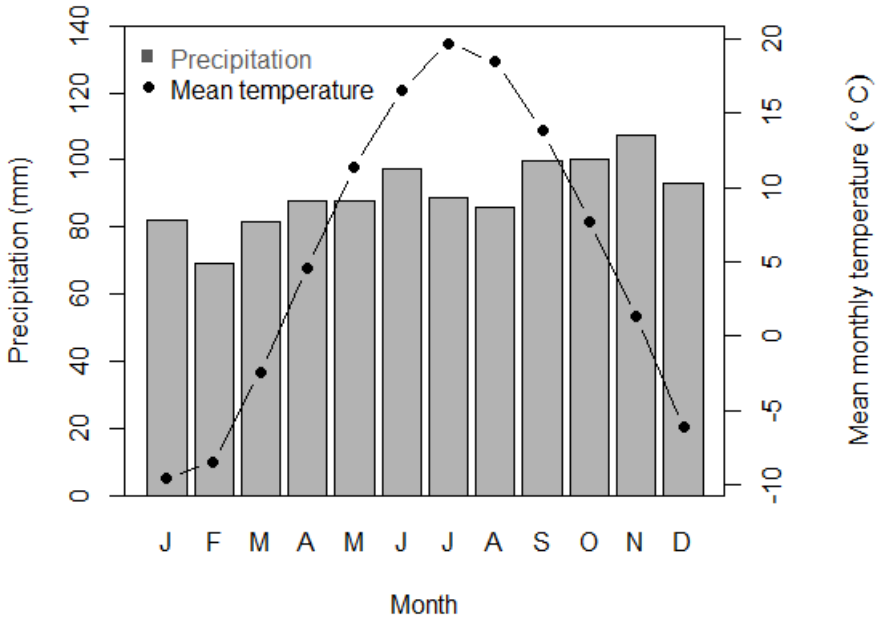

Figure 2.1: Climate summary for Howland Forest, Maine from the interpolated PRISM gridded climate dataset from 1895-2105.

2.2.3 Data collection

We measured tree growth on a large mapped stem plot established by the Laboratory for Terrestrial Physics at NASA's Goddard Space Flight Center for remote sensing and ecosystem dynamics research (see Weishampel et al. 1994; Ranson et al. 2001; Sun et al. 2011). In 1989, all trees 3.0 cm and larger at breast height (DBH) were mapped and measured in the 3-ha forest plot (150 m x 200 m), recording ca. 7,800 stems. Each tree was tagged using a unique identification number. This large mapped plot is subsequently referred to as the NASA plot.

In 2015 we re-measured all living and dead standing trees >10 cm at breast height (DBH, 1.37 m) in the NASA plot. We cored a subset of the re-mapped trees (ca. 10%), selected in a random stratified (by species and diameter class, using 10-20, 20-30, >30 cm classes) manner, resulting in 325 trees (Table 2.1). The selection reflected the size

distribution and abundance of each species in the NASA plot and represented trees across all canopy positions. We recorded the height, height to crown base, and canopy class for all trees in the subset. We extracted one increment core from each selected tree at breast height with a standard 5.2 mm (diameter) increment borer (Häglof Company Group, Långsele, Sweden). Cores were air-dried and secured to wooden mounts, then sanded and polished using increasingly fine sandpaper. We measured ring-widths to the nearest 0.01 mm using a Velmex sliding stage (Velmex Inc., Bloomfield, NY, USA) with MeasureJ2X software (VoorTech Consulting, Holderness, NH, USA) and stereomicroscope. We performed cross-dating using species-specific marker years, usually light or narrow rings, followed by statistical confirmation using COFECHA software (Holmes 1983).

Table 2.1: Species composition and sampling in the NASA plot. Total and Sampled refer to number of trees on the NASA plot.

Species	Total	Sampled	Percent Sampled
Red spruce (*Picea rubens*)	1395	142	10%
Eastern hemlock (*Tsuga canadensis*)	868	88	10%
N. white-cedar (*Thuja occidentalis*)	336	35	11%
Red maple (*Acer rubrum*)	281	31	11%
White pine (*Pinus strobus*)	153	17	11%
Balsam fir (*Abies balsamea*)*	65	8	12%
Yellow birch (*Betula alleghaniensis*)*	13	2	15%
Paper birch (*Betula papyrifera*)*	12	2	17%
TOTAL	3123	325	10.4%

*Excluded from individual species analyses due to low sample size

Tree ring measurements were used to back-calculate historical diameters for every year since NASA plot establishment in 1989. First, we estimated inside bark diameters using species-specific bark factors (Dixon and Keyser 2011). When possible, we adjusted ring-widths so that cumulative ring-width equaled half the inside bark diameter in 2015,

following methods and justification presented by Frelich (2002). Adjusted ring-widths compensate for off-center piths, but is only possible if cores include or approach the pith (<15 mm) and are not affected by central rot. We sequentially subtracted ring-widths from 2015 inside bark diameter to estimate each year's diameter inside bark. We then added predicted bark thickness back to each year's inside bark diameters for use in allometric equations. We also back-calculated heights using measured heights from 1989 and 2015. We assumed annual height growth reflected ring-width growth, and we calculated height increment by multiplying the total height growth by the ratio of ring-width to cumulative radial growth since 1989 (similar to methods presented by Kariuki 2002).

We estimated tree bole-mass for each cored tree from 1989 to 2015 using the updated Honer equations from Li et al. (2011) for all conifer species. Original Honer equations (Honer 1967), which have not been updated, were needed for hardwoods (representing less than 10% of trees). The Honer equations use height and outside bark diameter to estimate inside or outside bark volume. Corresponding heights and diameters for each year were used to estimate bole volumes with and without bark. The difference between inside and outside bark volumes was used to estimate bark volume. Volumes were multiplied by wood and bark specific gravities presented for each species in Miles and Smith (2009). For comparison, standardized tree-ring chronologies were also developed along with carbon mass increment to test climate–growth relationships; tree-ring series were standardized using dplR (Bunn 2008) using interactive detrending and a cubic spline with flexibility of 67 years for most trees.

We chose the 26-year period for our analyses to coincide with the year of the NASA plot establishment (1989). We refrained from extending our analyses further back in time due to potential uncertainties in predicting whole forest carbon mass increment. We acknowledge potential uncertainties arising from (1) unknown growth of trees that died

prior to 2015, becoming more of a limitation as we extend further back in time, and (2) the spruce budworm (*Choristoneura fumiferana*) outbreak (ending mid-1980's) confounding our analyses of climate-growth relationships.

2.2.4 Tree-level analysis

To test the tree-level climate response of each species, we developed a linear mixed-effects model with the response variable as tree-level annual carbon mass increment estimated from tree-ring series. To prevent model over-parameterization and avoid colinearity, we limited our predictors to two sets of climate variables. Climate variables included mean daily temperature and total precipitation, which were summarized for each season from 1988-2015 using the interpolated PRISM gridded climate dataset (Daly et al. 2008). Each season was characterized by three-month intervals beginning in the previous spring (pMAR-pMAY) to current fall (SEP-NOV), resulting in seven seasons for each climate variable. Tree-level variables included species, diameter, basal area, total stem mass, crowding, and elevation (a proxy for soils moisture), all of which are assumed to affect individual tree-level growth. All size metrics represent the previous year's size, and the crowding index was based on the 1989 inventory. The influence of crowding was estimated for each tree from Hegyi's (1974) index calculated from tree–tree distances and diameters, using a neighborhood radius of 10 m, as follows:

$$CI_f = \sum_{n=1}^{N} \left(\frac{S_n / S_f}{Distance_{nf}} \right)$$

where CI_f is the crowding index for the focal tree; N is the number of neighbor trees; S_n and S_f are sizes of neighbor and focal trees; $Distance_{nf}$ is the distance (m) between the neighbor and focal tree. Elevation was extracted from a detailed (50-cm gridded) digital elevation model.

We evaluated candidate models using corrected Akaike's information criterion (AICc) scores (subsequently referred to as AIC), which allowed us to determine which models were best supported by the data (Burnham and Anderson 2002). The seasonal climate variables and size variable that best fit the data were selected based on AIC values from others in the variable class. The selected variables from each variable class were tested along with crowding and elevation to determine the effect on the model. Each of the final variables was then tested for significant interactions with species and used to develop the final model. We used an autoregressive process to account for repeated measures from individual trees and temporal autocorrelation, expressed as 'tag' (i.e. unique tree identification) nested within year. The final model was also tested for spatial auto-correlation, and for meeting general assumptions of the mixed-effects model.

2.2.5 Species and stand-level analyses

Species and stand-level analyses were conducted using summed carbon mass increments from the cored trees. Our intent here was to determine how climate variability influences whole species growth (sum of carbon mass increments from individual members of that species) as well as the stand-level growth (sum of carbon mass increment from all individuals). Summed carbon mass increment maintains the signals from individual trees while homogenizing the effect of tree-level factors like size and crowding. We used bootstrapped response function analysis (see Biondi and Waikul 2004) to test species and stand-level response against eight climate variables (Table 2.2) for all months from the previous March to current September (except for growing degree days and snowfall, for which only applicable months were used). The PRISM gridded climate dataset (Daly et al. 2008) was used for monthly temperature and precipitation. Potential evapotranspiration was calculated using methods presented by Hargreaves and Samani (1982). Growing degree days were calculated using a baseline temperature of 5º C.

Monthly snowfall data was obtained through the NOAA Climatic Data Center (Menne et al. 2012) at the Millinocket airport station (approximately 48 km north of the research site). Stream flow from the Penobscot River at West Enfield was collected through the USGS National Water Information System from 1988-2015 (U.S. Geological Survey 2012). The full list of climate variables used for the analysis are presented in Table 2.2.

Table 2.2: Climate variables used for species and stand-level analyses.

Variable	Abbreviation	Units
Average maximum daily temperature	tmax	°C
Average mean daily temperature	tmean	°C
Average minimum daily temperature	tmin	°C
Growing degree days	gdd	degrees over 5°C
Total monthly precipitation	precip	mm
Total monthly snowfall	snow	mm
Precipitation over potential evapotranspiration	P/PET	mm
Streamflow (Penobscot River at Enfield)	flow	m^3/sec

2.3 Results

2.3.1 Tree-level analysis

Seasonal climate and size variables were selected based on AIC values compared to others within the same variable class, shown in Table 2.3. For both precipitation and temperature, values from the previous summer produced the strongest models, followed by previous fall precipitation and spring temperature from each class. Square root transformed stem mass was the best performing size variable, fitting the data better than other transformed and non-transformed size metrics.

Table 2.3: Variable selection within variable class (seasonal precipitation, seasonal temperature, previous year size). ΔAIC = model AIC difference from the top model.

Variable Class / Variable	ΔAIC
Seasonal precipitation (precip)	
Previous summer	0
Previous fall	65.6
Summer	119.0
Winter	183.0
Previous spring	235.9
Spring	246.3
Seasonal temperature (temp)	
Previous summer	0
Spring	64.6
Winter	72.4
Previous spring	124.7
Summer	136.8
Previous fall	159.2
Previous year size (size)	
√Stem mass	0
Stem mass	38.2
Diameter	68.8
√Basal area	68.8
√Diameter	70.9
Basal area	83.8

The best supported variables representing precipitation, temperature, and size (above) were then combined with crowding, and elevation to determine which were most suitable for the overall model (Table 2.4). Elevation contributed very little to the model, and was therefore excluded from further analysis. The four remaining variables (representing precipitation, temperature, size, and crowding) were meaningful predictors, and each showed significant interactions with species. We evaluated the full model by sequentially removing each variable and interaction from the model to determine the relative contribution (Table 2.5). The full final model was constructed using the four variables (representing precipitation, temperature, size, and crowding), each with species interactions. The model had a marginal $r^2 = 0.57$ (representing the variance explained by

fixed factors) and a conditional $r^2 = 0.83$ (representing the variance explained by random and fixed factors). The final model did not display spatial autocorrelation, and satisfied the assumptions of constant variance and independence.

Table 2.4. Variable selection between variable classes. Variable abbreviations are shown in parentheses. ΔAIC = model AIC difference from the top model.

Variables	ΔAIC
Previous summer precipitation (precip)	0
Previous summer temperature (temp)	89.0
√Stem mass (size)	115.3
Hegyi crowding index (crowd)	197.5
Elevation	234.1
Null model	246.5

Table 2.5: Model selection based on four variables and their interactions with species. To illustrate the relative contribution of each individual variable, each was removed from the full model (top row), and the AIC values are presented. ΔAIC = model AIC difference from the top model.

Variables	ΔAIC
spp*size + spp*temp + spp*precip + spp*crowd	0
spp*temp + spp*precip + spp*crowd	76.3
spp*size + spp*temp + spp*precip	102.5
spp*size + spp*precip + spp*crowd	179.6
spp*size + spp*temp + spp*crowd	221.9
spp	639.3

The effect of each variable × species interaction on carbon mass increment is plotted in Figure 2.2 through Figure 2.4, keeping the other variables in the model constant at their respective means. Note the size of the confidence interval is in part due to tree-to-tree variability, but also reflects relative abundance (more common species had larger samples). Red spruce and eastern hemlock were the most abundant and therefore had the smallest confidence intervals.

White pine not only showed dramatically greater growth, it responded to climate differently than did other species (Figure 2.2). White pine responded favorably to increases in previous summer temperature and precipitation. Other species either responded negatively (eastern hemlock and red spruce), or were indifferent to previous summer temperature (red maple and northern white-cedar). Red spruce and eastern hemlock both responded favorably to summer precipitation (as seen in white pine), but northern white-cedar and red maple again showed very weak associations. Based on this information alone, we would assume red spruce and eastern hemlock have similar summer climate preferences, while red maple and northern white-cedar both show indifference to previous summer climate.

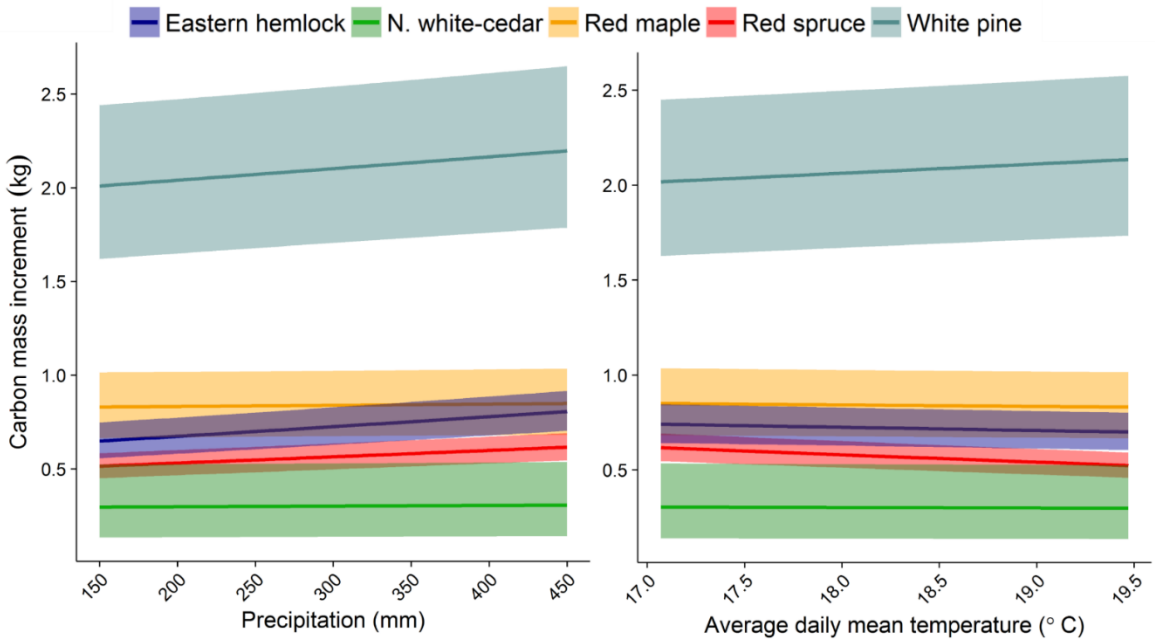

Figure 2.2: Model results depicting the effect of climate on carbon mass increment with other climate variable, size, and crowding held at their respective means. The shaded portions represent the standard errors from the fitted model.

As expected, our data show a positive association between stem mass (a size metric) and annual carbon increment (Figure 2.3). White pine accumulated carbon mass

faster than did any other species across all sizes. The model showed small eastern hemlocks had the slowest growth of any species, but the rate of carbon mass increment for this species increased with trees of higher mass, exceeding red spruce and northern white-cedar at large sizes. Red maple maintained relatively fast growth across sizes, increasing at a rate similar to that of red spruce.

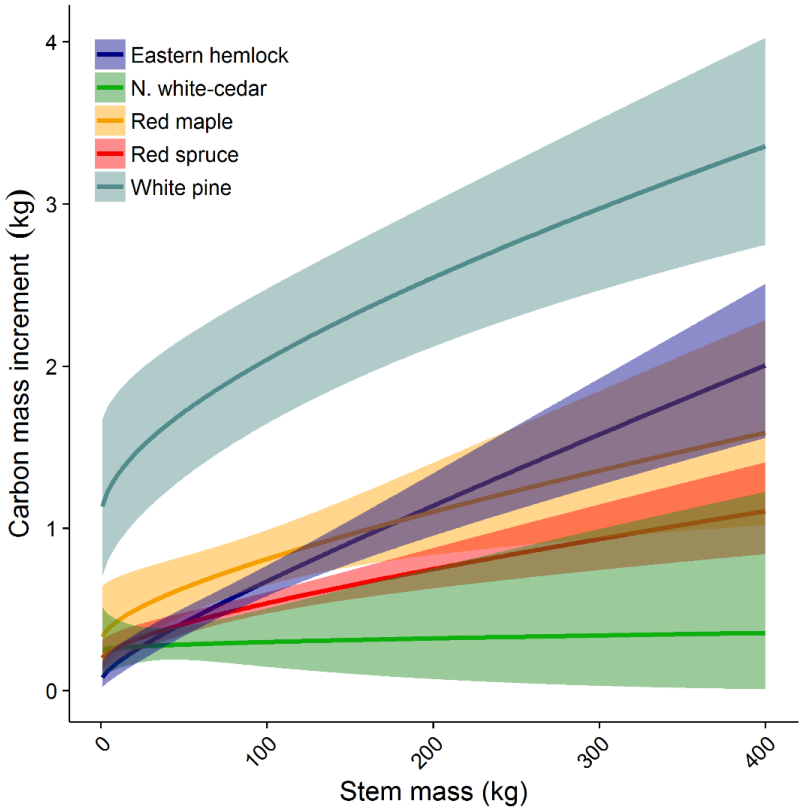

Figure 2.3: Model results depicting the effect of tree size (expressed as stem mass) on annual carbon mass increment, based on model simulations holding climate and crowding variables at their respective means. The shaded portions represent the standard errors from the fitted model.

Our data show a negative association between carbon mass increment and the Hegyi crowding index (Figure 2.4) for all species. At intermediate levels of crowding, eastern hemlock and red maple appear to be slightly less sensitive to crowding than are red spruce and northern white-cedar. The influence of crowding is emphasized in white

pine growth: trees displayed their enormous growth potential under low crowding but under high crowding, they were comparable to other species.

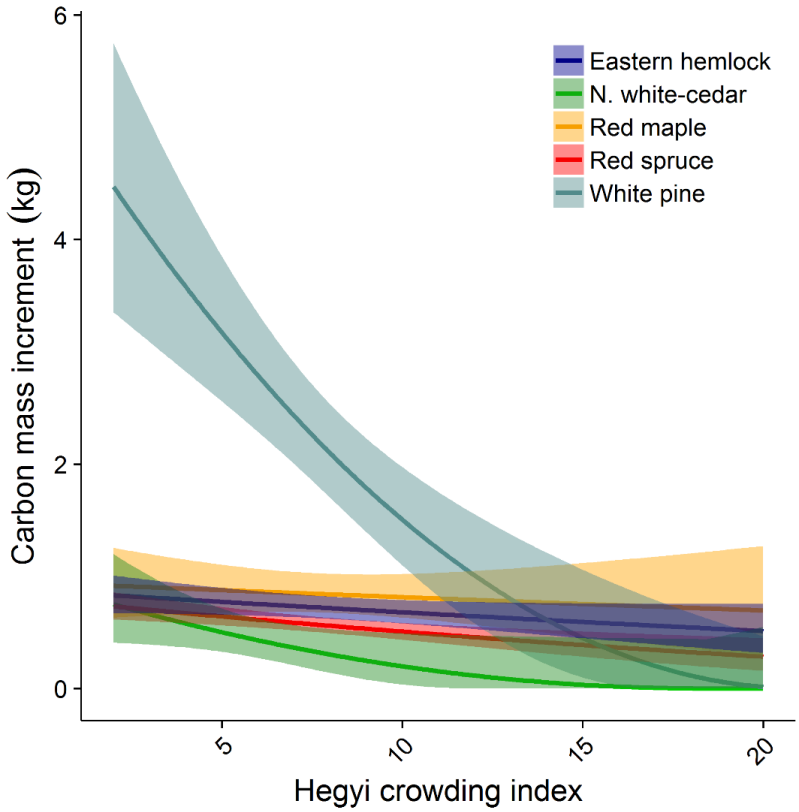

Figure 2.4: Model results depicting the effect of crowding on carbon mass increment with climate variables and size held at their respective means. The shaded portions represent the standard errors from the fitted model.

2.3.2 Species- and stand-level analyses

Species-level carbon mass increment (presented in Figure 2.5) represents the relative contributions of each species to stand-level carbon sequestration. Species displayed different magnitudes of carbon mass increment and unique year-to-year variability. Red spruce represents the greatest proportion of stand-level carbon gain over much of the study period, which is not surprising given that this species represents roughly half of the sampled trees. In recent years, however, carbon mass increments for white

pine and eastern hemlock have at times surpassed red spruce increments. This trend is particularly striking for white pine: despite representing only 5% of the total stems, in recent years it has contributed to stand-level growth at a rate roughly equivalent to that of the two dominant species (Figure 2.6). We see prominent long-term trends for two most abundant species; eastern hemlock shows an overall increasing trend over the time series, while red spruce growth is declining. Additionally, the average annual carbon increment and variability for individual trees are presented in Figure A.3 and Table A.3 in the Appendix.

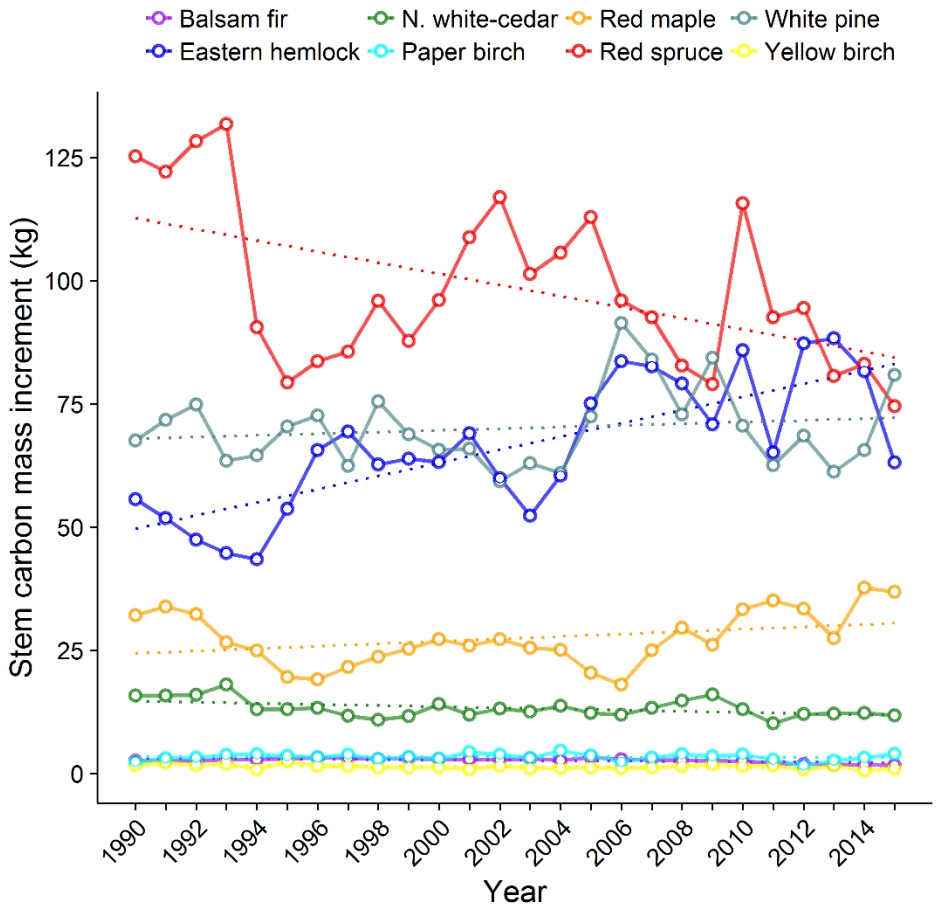

Figure 2.5: Species-level carbon mass increment over the 25-year study period. Data represent summed carbon mass increments from a stratified random selection of trees. Note the decline in red spruce and increase in eastern hemlock. Fitted linear regression lines (dotted) shown to emphasize overall growth trends.

The summed carbon mass increment from all cored trees showed striking year-to-year variability (Figure 2.6), exhibiting a steep decline in the early 1990's followed by a gradual increase until 2010, and a small decline in recent years. This year-to-year variability was used to determine which climate factors have the largest effect on stand-level carbon gain.

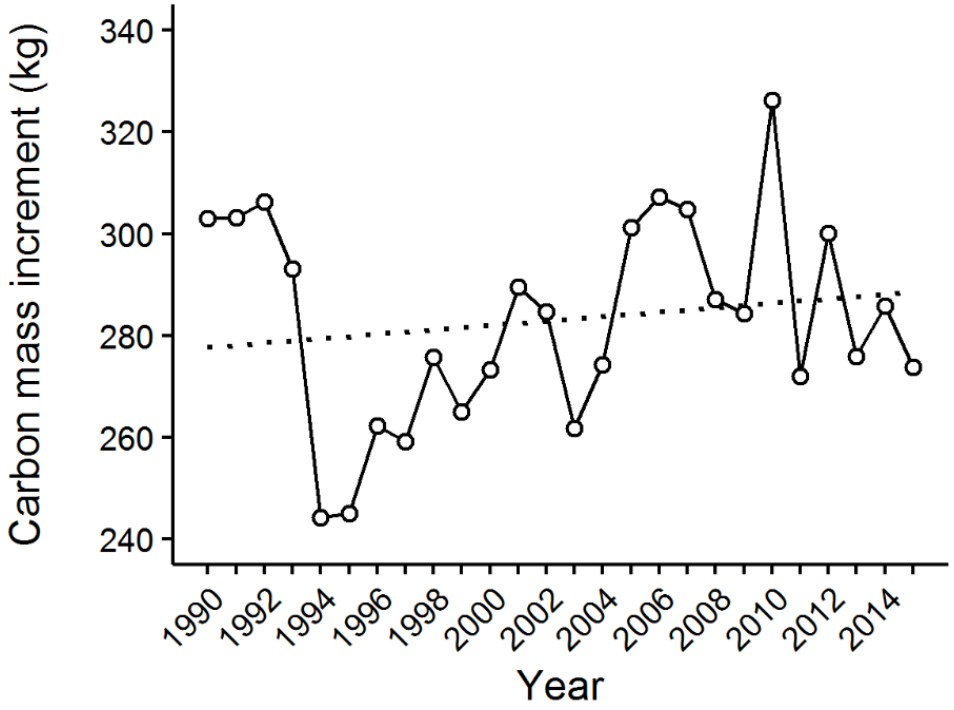

Figure 2.6: Stand-level annual carbon mass increment estimated by summing increments from a stratified random selection of trees on the NASA plot. Fitted linear regression line (dotted) shown to emphasize overall growth trend.

Results from species- and stand-level response function analysis for all climate variables clearly highlight the differential responses among species (Table 2.6, Figure 2.7, and Figure 2.8). Red spruce responded negatively to previous summer temperatures (i.e., lower growth with higher temperatures), and showed no significant responses to precipitation. Eastern hemlock, the second most abundant species, responded favorably to previous fall temperatures and winter precipitation (i.e., greater growth with higher

temperature and precipitation). White pine demonstrated a positive association with spring, and negative association with summer temperatures, but no monthly temperature variables were significant. Previous season precipitation (July and November) was positively associated with white pine growth. In general, previous-year growing-season climate variables were more influential on growth than were current-year variables.

We compared results from our carbon mass increment approach to those of typical species-level dendrochronology techniques using chronologies developed from standardized ring width. Visual comparisons between the two demonstrate similar high-frequency variability, but standardized chronologies did not retain low-frequency variability present in carbon mass increment (Figure A.2 in the Appendix). Species-level response function analyses showed the two metrics had similar monthly relationships, but resulting significant response variables differed between the metrics. Significant variables from the ring-width response function analyses are presented in Table A.4 (in the Appendix).

Table 2.6: Species-level response function analysis summary (n=number of trees). The prefix *p* indicates previous year variable.

	n	tmean	tmax	tmin	gdd	precip	snow	P/PET	flow
Red spruce	142	-pJUL	-pJUL	-pJUL	-pJUL	-	-	-	-
Eastern hemlock	88	+pOCT	-pMAY +pOCT	-	-	+FEB	-	-	-
White pine	17	-	-pMAR	-	-	+pJUL +pNOV	-	+pNOV	-MAR
N. white-cedar	37	-SEP	+pMAY	-SEP	-SEP	-	-	-	-
Red maple	31	-	-	+AUG	+pMAY	-	-	+pAUG +pDEC	-
Stand-level	325	+APR	+JAN	+APR	+APR	+pAUG	-	+pAUG	-

tmean: Average daily mean temperature

tmax: Average daily maximum temperature

tmin: Average daily minimum temperature

gdd: Total growing degree days

precip: Total precipitation

snow: Total snowfall

P/PET: Precipitation over potential evapotranspiration

flow: Stream flow

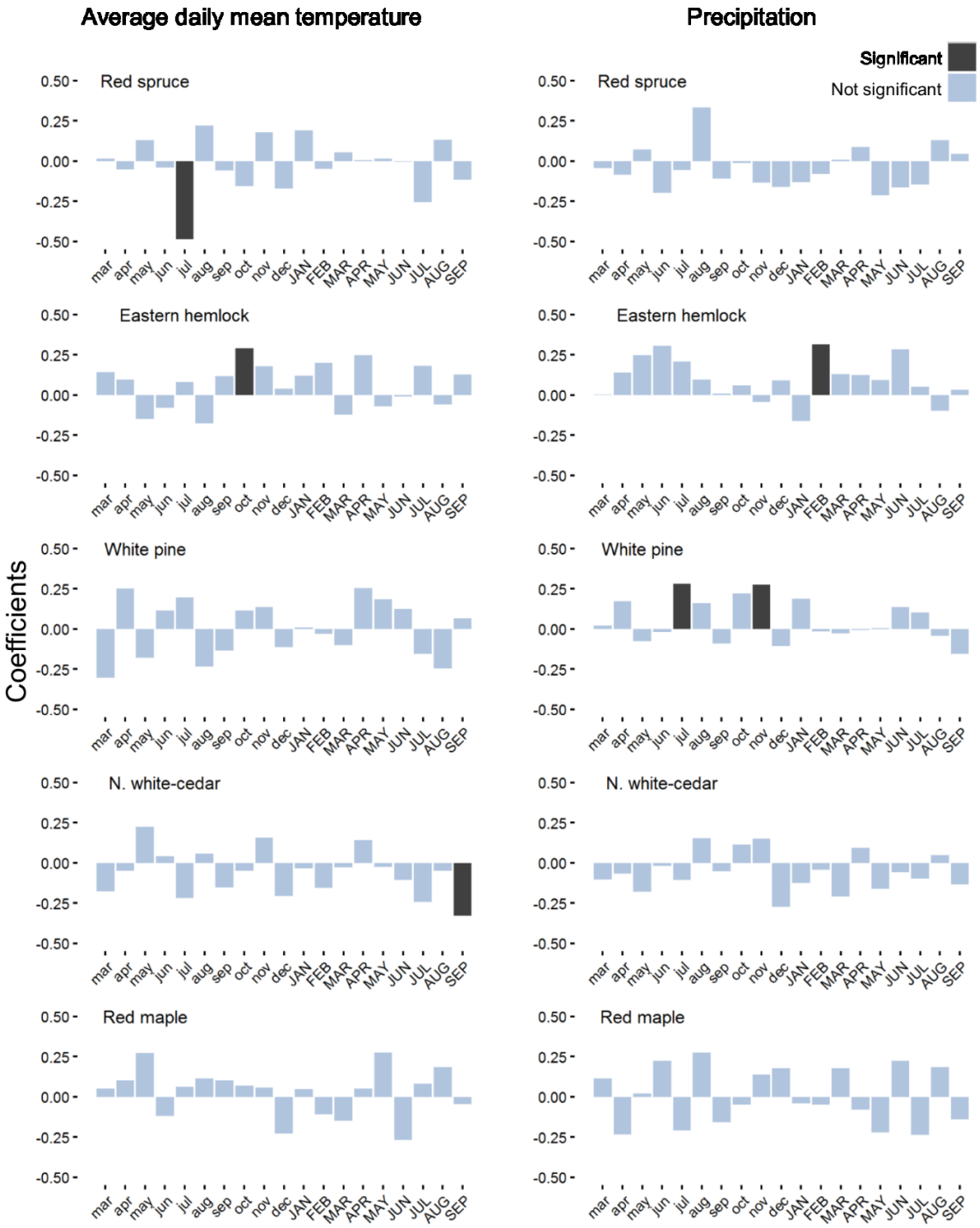

Figure 2.7: Species-level growth response (based on carbon mass increments) to mean temperature (column 1) and precipitation (column 2) for all months from previous March to current September. Previous months in lower case; current months in upper case.

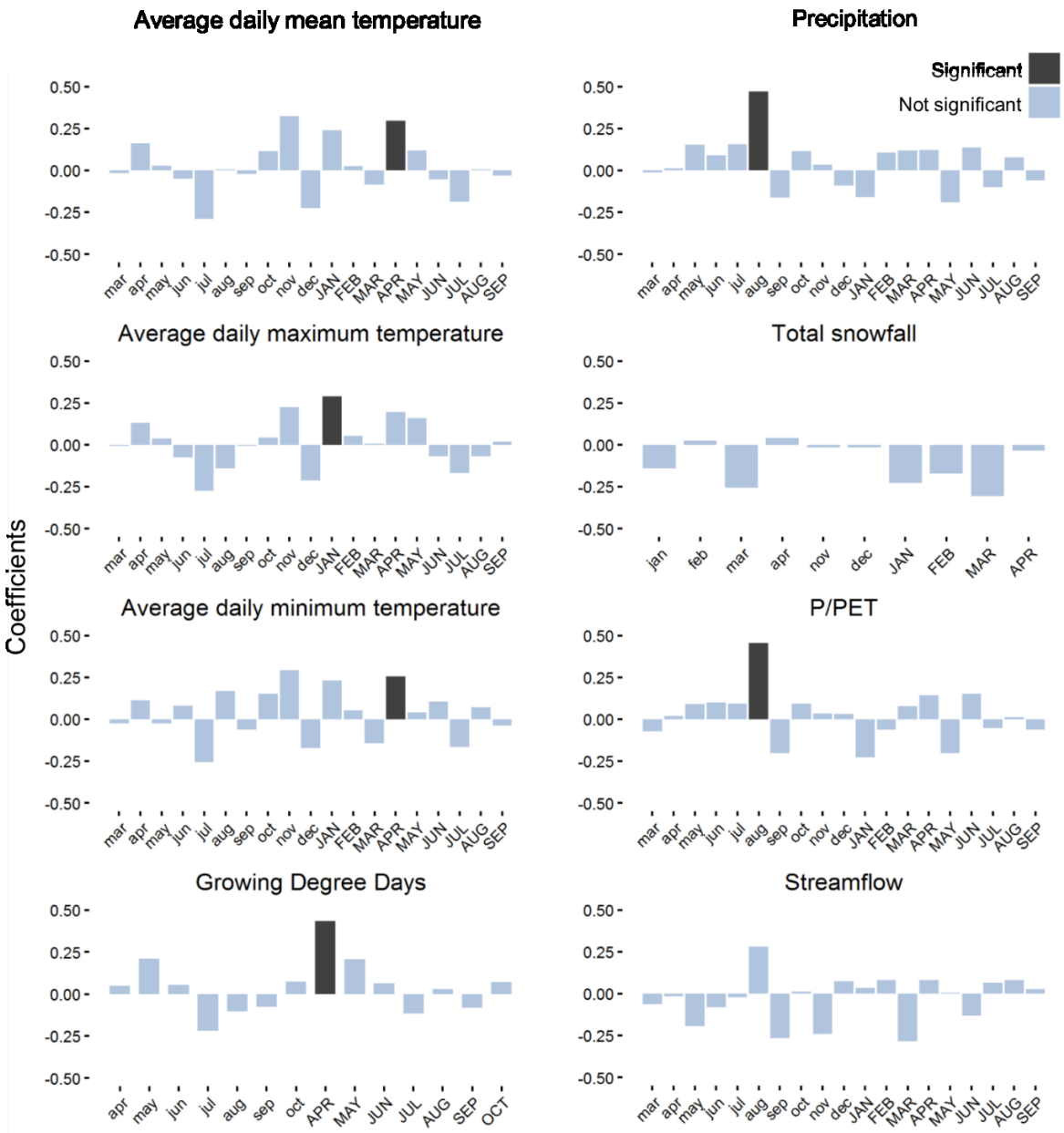

Figure 2.8: Stand-level growth response (based on cumulative carbon mass increment) to all climate variables. Previous months in lower case; current months in upper case.

2.3.3 Climate summary

Climate data used for the analyses above are summarized in Figure 2.9. The climate data indicated changing conditions for both precipitation and temperature. The seasonal precipitation showed an increasing trend for all seasons except spring, indicating the climate at Howland Forest is becoming wetter over time. All seasonal mean temperature series also display gradual increasing trends over the past 25 years.

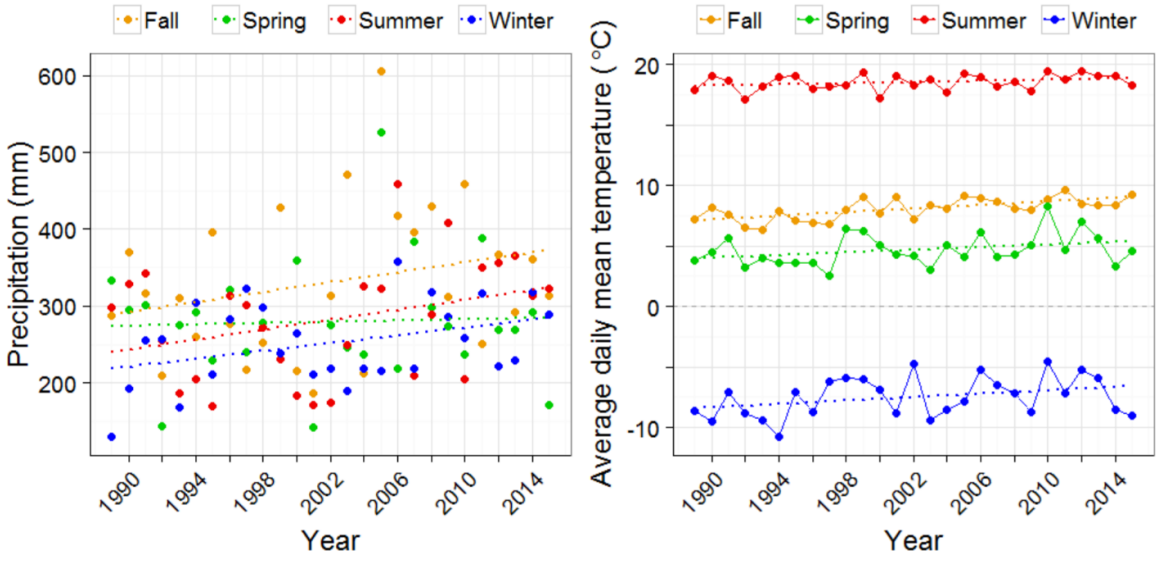

Figure 2.9: Climate trends at Howland Forest from 1989 to 2015 represented in total seasonal rainfall and seasonal mean daily temperature. Seasons were summarized in three month intervals, starting with winter summarized from previous December to February.

2.4 Discussion

In the current chapter, we explored methods to identify climate-growth relationships for individual trees, species, and an entire forest stand. Our analyses of individual trees demonstrated that two tree-level variables (i.e., size and crowding) contributed significantly to growth variability. We present species- and stand-level climate-

growth relationships using carbon mass increment from a random and representative sample of the population. We tested monthly climate variables on carbon mass increment using response function analysis. Summing carbon mass increment from several trees homogenizes the influence of tree-level factors (i.e. crowding and size), and combines the total effects of climate signals, weighting trees based on their relative contributions to total carbon increment. We believe these analyses represent a valid and novel method for testing the effects of climate on stand-level growth.

2.4.1 Tree-level analysis

The variable selection process suggested previous summer variables are the best seasonal climate predictors for modeling carbon mass increment from individual trees at Howland Forest. In the full model, previous summer precipitation was positively associated with growth of red spruce, eastern hemlock, and white pine. Other studies have demonstrated positive relationships between previous summer precipitation and growth of red spruce (Conkey 1979) and eastern hemlock (Cook and Jacoby 1977; Cook and Cole 1991). Previous summer temperatures had differential relationships among species; high temperatures were associated with lower carbon increment for spruce and hemlock but higher carbon increment for white pine. Warm temperatures have been shown to have damaging effects on red spruce productivity (Vann 1994; Day et al. 2000) and may reduce forest productivity of the entire region (Mohan et al. 2009). Neither previous summer climate variables demonstrated negative effects on northern white-cedar or red maple growth. Aside from their known complacency to climate, these species tended to grow in relatively wet areas within the plot, suggesting they are less prone to summer water limitation. While previous summer climate variables performed better than other seasonal summaries, they are clearly not the only climate variables affecting carbon increment. The

variable selection process also suggested previous fall precipitation and spring temperature, as they may be predictors worth further investigation.

Tree size was an important predictor for annual carbon mass increment, demonstrating that larger trees accumulate mass at a faster rate than smaller trees (as in Stephenson et al. 2014). Our data suggested stem mass is a better predictor than diameter or basal area at breast height. Many of the species used for this analysis are considered shade-tolerant, but each species demonstrated unique growth patterns according to size. Red spruce, eastern hemlock, and northern white-cedar are considered very shade-tolerant species (Baker 1949) capable of surviving long periods of suppression with very slow growth (Johnson and Abrams 2009). The ability to survive in the understory is apparent for these species, accumulating very little mass at small sizes (Figure 2.3). Red spruce and eastern hemlock showed periods of suppressed growth at small sizes, followed by increasing carbon accumulation at larger sizes. Eastern hemlock growth displayed the most prominent increase in growth with tree size, perhaps suggesting growth releases at earlier developmental stages at Howland Forest. Northern white-cedar tended to remain slow growing throughout all sizes, and had a large variability between trees. White pine and red maple had high initial and sustained growth rates. Emergent white pines showed notably fast biomass growth even at large sizes. Red maple, regarded a shade-tolerant hardwood, showed a fast initial phase of carbon gain and steady increase with increasing size. These growth patterns, suggesting rapid growth following a period of suppression, reflect the ecology of the spruce dominated stands in the region, and compliment historical accounts of the species (Fajvan and Seymour 1993; Fraver and White 2005).

Our data indicated crowding had a negative effect on carbon mass increment for all species, but that sensitivity to crowding may vary between species. As expected,

incorporating spatially derived crowding information improves our model predictions (Canham et al. 2004, Fraver et al. 2013). Red spruce and eastern hemlock showed gradually decreasing carbon accumulation with increasing crowding, while northern white-cedar showed a dramatic growth reduction beyond moderate levels of crowding. White pine appeared to be far more sensitive than other species to crowding, emphasized by the enormous growth potential under low crowding, followed by a steep decline as crowding increased. It is unclear what factors are driving the species differences in crowding response. In addition to species differences, the effect of crowding may also vary with climate variables (Sánchez-Salguero et al. 2015), below-ground factors (Canham et al. 2004), species composition of neighbors (D'Amato and Puettmann 2004), and tree size (Das 2012).

Modeling the effects of climate in this manner allowed us to take advantage of a large number of sample years (8100+ tree rings) to test climate-growth relationships. The model allowed us to incorporate non-climatic data to account for additional variability between trees and therefore improve predictions. However, this type of model is restricted by the number of climate variables we can include, due to colinearity. In addition, interactions between variables add complexity and make model interpretation difficult. Although size and crowding variables provide interesting supplemental information, we refrain from detailed analysis comparing variable importance and additional interactions besides species.

2.4.2 Species-level analysis

The species-level contributions of carbon mass increment indicated a shift in forest carbon dynamics at Howland Forest over time. Based on the high abundance of red spruce, we expected the species to maintain the highest carbon mass increment throughout the time series. However, a decline in red spruce and increase in hemlock

resulted in a convergence with white pine carbon mass increments, suggesting these three species were roughly equal in annual carbon gain as of 2015 (Figure 2.5). White pine and red maple displayed relatively stable annual productivity with little evidence of increasing or decreasing trends. Northern white-cedar, similarly to red spruce, had a decreasing trend since 1990 (Figure A.2 in the Appendix). Projecting these long-term trends into the future suggests a potential shift in carbon sequestration dominance from red spruce to eastern hemlock at Howland Forest.

The large annual carbon mass increment of white pine despite the small number of individuals was a striking finding. Although white pine was markedly less abundant than other trees species (representing only 5% of the stems), individuals on the NASA plot were the fastest growing in terms of diameter, basal area, and carbon mass. White pine has also shown an increasing number of tree sized individuals over the sampling period (1989-2015) shown in Table A.1 in the Appendix. If the large individual white pines maintain this growth rate, and others are recruited to dominant canopy positions, they will continue to contribute a substantial portion to stand-level carbon increment at Howland Forest.

The annual carbon increment summaries were used to identify climate factors most strongly affecting carbon mass increment of each species (Table 2.6). Red spruce consistently responded negatively to previous July temperatures (the warmest month of the year). Other studies have demonstrated the negative growth response of red spruce to previous summer temperature (Conkey 1979). Eastern hemlock did not appear to be sensitive to previous summer temperature in the species-level analysis, but responded positively to previous October temperatures. The southerly distribution of eastern hemlock may indicate the species is more resistant to high summer temperatures than is red spruce. The relationship between eastern hemlock growth and October temperatures

could suggest the species takes advantage of cool late-season temperatures for photosynthesis (also higher light availability following leaf loss of deciduous tree species). It is unclear if gradually increasing trends in both summer and fall temperatures at Howland Forest (Figure 2.9) alone are responsible for the dramatic growth trends seen in red spruce or eastern hemlock, or if they are simply correlated with them over time. Climate clearly influences stand-level productivity (Keenan et al. 2014), and has been shown to differentially affect co-occurring species (Friedrichs et al. 2009; Miyamoto et al. 2010). Therefore it is possible climate has a role in the differential trends seen in species-level carbon accumulation.

2.4.3 Stand-level analysis

The cumulative carbon mass increment for all species (Figure 2.6) showed significant positive responses to previous summer precipitation and early season temperature variables (Figure 2.8). Positive relationships with August precipitation and P/PET indicate trees may be periodically limited by water availability in summer. Water stress in trees may reduce current year photosynthesis rates, which could affect current and following year growth (Körner 2003). Prolonged periods of water stress can have lasting effects on tree growth, extending into the following year or several years later (Anderegg et al. 2015). Drought conditions may be responsible for the low productivity in 1994 and 1995, as summers 1993-1995 displayed below average precipitation (Figure 2.9).

Overall, stand-level productivity showed a slight increase over time, with the maximum carbon mass increment in 2010. April (mean daily, minimum daily, and growing degree days), and February (maximum daily) temperatures all showed significant positive relationships with stand-level productivity. The relationship with April temperatures are similar to previous studies suggesting cool-weather conifers are limited by spring

temperature (Rossi et al. 2008). The productive year in 2010 was an unusually warm spring, which supports the suggested relationship with April temperature. Further, data collected using the eddy-covariance technique have shown that above average spring temperatures have a positive effect on forest productivity at several New England forest types (Hollinger et al. 2004; Richardson et al. 2010; Keenan et al. 2014).

2.4.4 Level summary

Results from across the three organization levels (individual trees, species, and the stand) reveal several consistencies in climate-growth relationships. Tree-level and stand-level analyses both potentially indicate a water limitation during the previous summer. The highest transpiration rates occur during the summer (Catovsky et al. 2002) and therefore this season exerts the highest water stress on trees. Water stress affects photosynthetic efficiency by causing partial stomata closure and reduced carbon assimilation (Zweifel 2006). We see that despite receiving relatively high rainfall (>1000 mm / year), these species appear to be periodically limited by water availability. For this reason, the increasing summer precipitation trends (Figure 2.9) may have a positive effect on tree growth.

Tree-level and species-level analyses showed consistent negative growth response by red spruce to previous summer temperatures. Spruce sensitivity to high temperature has been documented for numerous *Picea* species (Wilmking et al. 2004; Miyamoto et al. 2010; Aakala and Kuuluvainen 2011), including red spruce specifically (Conkey 1979; Vann et al. 1994; Day et al. 2000) and the closely related black spruce (Walker and Johnstone 2014; Gewher et al. 2014; Girardin et al. 2015). These studies corroborate our finding that red spruce exhibited reduced growth when experiencing above-average temperatures. Red spruce may be the region's first indicator of a forest change due to warming, and continued increase in summer temperatures would imply

continued decline of red spruce in the future. Species-level associations with previous summer precipitation are consistent for both tree- and species-level analyses, but species-level relationships to previous summer temperature response are more tenuous between the two analyses.

Results from species- and stand-level analyses did not identify any shared statistically significant monthly climate variables, but the significant stand-level variables responded consistently (i.e. positive or negative response) across species-level analyses (Figure 2.7). Interestingly, the sum of all individual species responses (used to develop stand-level response) emphasized previous summer precipitation and spring temperature as the climate factors most broadly affecting individual tree growth. We may expect stand-level productivity to be stabilized by species diversity (Isbell et al. 2015), making it less sensitive to climate than that revealed by species-level analyses. However, despite being stabilized by the combined growth of many species, we see significant growth responses to simple measures of temperature and precipitation at the stand-level.

2.4.5 Potential limitations

Although we believe our sampling strategy is representative of the forest type at Howland, the carbon mass increment responses are heavily influenced by large trees. This natural weighting system was used to capture the annual variability in whole forest carbon sequestration. As we have shown, large trees accumulate disproportionately more mass than smaller trees (Figure 2.3), and therefore have a larger influence on landscape level carbon gain. Previous studies have shown that large diameter trees may have a higher water demand than small trees (Mérian and Lebourgeois 2011; D'Amato et al. 2013). Our results, suggesting water stress could have a noticeable negative effect on stand-level tree growth, may be skewed by the effect on large trees. While these methods

may be useful in understanding stand-level carbon increment, they are not necessarily applicable for generalizations across individual trees.

The low number of individuals of several species may limit the interpretation of our results. Inferences regarding white pine in particular are somewhat limited due to the relatively low sample size. The large discrepancy between annual carbon mass increment of white pine and all other species makes this species particularly important in terms of carbon mass increment. Our tree-level analyses would benefit from a larger sample of white pine, and to a lesser extent red maple and northern white-cedar.

Finally, interpretation of our species-level results may have been influenced by long-term trends of carbon mass increment, potentially independent of climate. Eastern hemlock shows an increasing trend over the time-series, as fall temperatures have concurrently increased over the period. It is unclear whether the increase in eastern hemlock is caused by a change in temperature or some other stand attribute. An age-related increase or decline in stand level carbon increment could be problematic when testing climate relationships over long periods.

2.5 Conclusions

Our methodologies explored the use of carbon mass increment as an alternative to traditional tree-ring chronologies to analyze climate–growth relationships. We implemented this technique to help clarify climate response of a multi-aged, mixed-species forest. We tested the applicability of annual carbon mass increment to detect climate response at the tree-, species-, and stand levels. We believe annual carbon mass increment is more appropriate than traditional dendrochronological techniques in complex forest systems. By collecting a large unbiased sample, we tested whole forest sensitively to climate and observed long-term trends in forest productivity.

Using carbon mass increment, we demonstrated stand-level growth can be sensitive to a different set of climate variables than those affecting individual species. We documented previous summer precipitation and spring temperature as the most influential variables affecting stand-level growth at Howland Forest. Deficits in previous summer (August) water availability may limit the efficiency of photosynthesis and affect the amount of non-structural carbohydrate storage available for the following season's growth (Körner 2003). A positive relationship between spring (April) temperature and stand-level carbon increment corroborates previous studies linking increasing spring temperatures to early leaf-out phenology (Morin et al. 2009, Polgar and Primack 2011) and higher annual carbon uptake (Black et al. 2000; Hollinger et al. 2004; Richardson et al. 2009, Keenan et al. 2014). According to these studies, our explanations of stand-level response seem plausible, and have biological justification. Testing the applicability of this technique at other stands could provide further validation.

These and other long-term datasets at Howland Forest (see Chapter I) suggest an increasing trend in annual forest productivity. In forests not limited by water, climate change may have positive effects on forest productivity (see Boisvenue and Running 2006). Increased productivity in most cases infers forest health, but our results suggest this increase may be occurring at the expense of reduced growth for certain species. That is, our study shows declines in red spruce and northern white-cedar growth since 1990. Under warming trends, we would expect red spruce growth decline due to its sensitivity to high-temperatures (Vann et al. 1994). The sensitivity of spruce has led to projected spruce–fir habitat declines resulting from climate change (Iverson et al. 2008). Slow-growing species (i.e. red spruce, northern white-cedar) may have difficulty competing with relatively fast-growing species adapted to warmer climates. Our study demonstrates a divergence between species, suggesting declines in red spruce growth and increases in

eastern hemlock may be an early indication of a change occurring in species health of northern forests.

Maintained or increased stand-level productivity in lieu of species-level declines is possible due to a diverse mix of species with different climate-growth relationships. Maintaining high species diversity stabilizes ecosystem productivity by increasing resistance to climate extremes (Isbell et al. 2015). Climate conditions adversely affecting some species may have positive effects on others, resulting in higher stability and reliability of ecosystems (Naeem and Li 1997). Species diversity may become even more critical with increasing prevalence of insect pests and disease resulting from a changing climate (Dymond et al. 2014). We see evidence of productivity stabilization from our mixed species stand, illustrated by other species compensating for lower red spruce productivity, resulting in a relatively stable and even increasing stand-level productivity. If tree species diversity contributes to forest resiliency, within species variability may have a similar effect on stabilizing forest productivity in response to climate. Tree size and canopy position may provide heterogeneous climate response (as seen between species), and therefore provide additional stability to stand-level productivity. Using this reasoning, we would expect complex, multi-aged, multi-strata forests to be more resilient to climate change than even-aged stands.

In summary, Howland Forest's increasing stand-level productivity shows little evidence of stress from recent temperature and precipitation trends. Instead, annual carbon gain appears to be increasing. However, analysis on the species-level suggests there may be underlying stressors causing long-term growth declines of certain species. If trends continue, and these stressors ultimately result in tree mortality, we may see sustained declines in stand-level production and increased carbon emissions from decomposition for many years. The future growth of red spruce may provide many

valuable clues into the effects climate change will have on this region's ecological communities.

EPILOGUE

This study has succeeded in furthering our knowledge of forest carbon dynamics. We addressed the link between two prominent metrics of forest productivity (tree growth and CO_2 flux) and demonstrated that trends in tree growth at times lag behind those in CO_2 sequestration. We identified climate factors affecting woody biomass production, and explored novel strategies to test climate–growth relationships. However, more research is needed to fully understand mechanisms of tree carbon sequestration and storage, as well as factors affecting their year-to-year variability. Addressing carbon allocation on an annual basis is incredibly difficult because of transport, storage, and mixing of non-structural carbohydrates. Exploration using methods mentioned below would help further our understanding of the physiological aspects of carbon allocation, and clarify the results we report.

Important knowledge gaps exist in understanding trade-offs between storage and growth, and how carbon allocation strategies change on an annual basis. Understanding within-year variability in tree growth as well as CO_2 flux could reveal additional clues to the growth limitation theory, which states that growth is not necessarily limited by carbon supply, instead may be limited by suitable conditions for wood formation (Körner 2003). We provide additional evidence that the yearly onset and termination of wood formation is cued by different environmental drivers than those controlling photosynthesis (Körner 2015). However, we still do not know what controls the amount of resources allocated to storage, nor how allocation strategies differ between plant species (Hartmann and Trumbore 2016). Allocation to storage is expected to be mediated by nutrient and water availability, but the mechanisms for regulating carbon allocation are still poorly understood (Dietz et al. 2014).

Determining age of non-structural carbohydrates from carbon isotope tracers (^{14}C) can also clarify many questions we have about carbon allocation strategies (Epron et al. 2012). Multiage reserves commonly contribute to normal tree functions, which suggest a mixing of stored and current-year fixed carbon (Hartmann and Tumbore 2016). The ability for non-structural carbohydrate stores to remain in trees for over a decade (Richardson et al. 2013) is somewhat problematic when attempting to link tree growth to specific timeframes of CO_2 flux or climate data. Using isotopes to determine age of non-structural carbohydrates in newly assimilated tissue could clarify this topic (Keel et al. 2006). However, the nature of allocation patterns would suggest these relationships remain dynamic and difficult to generalize.

Finally, using diameter growth to estimate total tree growth (as we did in this study) does not account for variability in production of other plant biomass, including fine roots, needles/leaves, litter, or reproductive efforts. Various plant tissues likely require carbohydrate inputs at times of the year different than those required for diameter growth. Studies concerning specific climatic effects on needle production (Hennessey et al. 1992), fine root production (Finér et al. 2013), and reproductive effort (Roland et al. 2014; Moriera et al 2015) have shown that each sink responds to a specific set of climate drivers. The variability in resources allocated to these sinks, along with non-structural carbohydrate storage, clearly have an influence on the amount of resources available for diameter growth, and thus whole-tree wood production. Understanding these trade-offs would also be beneficial in understanding forest carbon allocation patterns.

REFERENCES

Aakala T, Kuuluvainen T (2011) Summer droughts depress radial growth of Picea abies in pristine taiga of the Arkhangelsk province, northwestern Russia. *Dendrochronologia*, **29**, 67–75.

Amiro BD, Barr AG, Barr JG et al. (2010) Ecosystem carbon dioxide fluxes after disturbance in forests of North America. *Journal of Geophysical Research*, **115**, 1–13.

Anderegg WRL, Schwalm C, Biondi F et al. (2015) Pervasive drought legacies in forest ecosystems and their implications for carbon cycle models. *Science*, **349**, 528–532.

Babst F, Bouriaud O, Papale D et al. (2013) Above-ground woody carbon sequestration measured from tree rings is coherent with net ecosystem productivity at five eddy-covariance sites. *New Phytologist*, **201**, 1289–1303.

Baldocchi D, Hinks B, Meyers T (1988) Measuring biosphere-atmosphere exchanges of biologically related gases with micrometeorological methods. *Ecology*, **69**, 1331–1340.

Baldocchi D (2003) Assessing the eddy covariance technique for evaluating carbon dioxide exchange rates of ecosystems: past, present and future. *Global Change Biology*, **9**, 479–492.

Baker F (1943) A Revised Tolerance Table. *Journal of Forestry*, 179–181.

Bakker JD (2005) A new, proportional method for reconstructing historical tree diameters. *Canadian Journal of Forest Research*, **35**, 2515–2520.

Barford CC, Wofsy SC, Goulden ML et al. (2001) Factors controlling long- and short-term sequestration of atmospheric CO2 in a mid-latitude forest. *Science*, **294**, 1688–1691.

Biondi F, Qeadan F (2008) A Theory-Driven Approach to Tree-Ring Standardization: Defining the Biological Trend from Expected Basal Area Increment. *Tree-Ring Research*, **64**, 81–96.

Biondi F, Waikul K (2004) DENDROCLIM2002: A C++ program for statistical calibration of climate signals in tree-ring chronologies. *Computers and Geosciences*, **30**, 303–311.

Black, T., Chen, W., Barr, A., Arian, M., Chen, Z., Nesic, Z., Hogg, E., Neumann, H., Yang P (2000) Increased carbon sequestration by a boreal deciduous forest in years with a warm spring. *Geophysical Research Letters*, **27**, 1271–1274.

Boisvenue C, Running SW (2006) Impacts of climate change on natural forest productivity – evidence since the middle of the 20th century. *Global Change Biology*, **12**, 862–882.

Bormann FH, Likens GE (1979) Catastrophic Disturbance and the Steady State in Northern Hardwood Forests. *American Scientist*, **67**, 660–669.

Bouriaud O, Bréda N, Dupouey J, Granier A (2005) Is ring width a reliable proxy for stem-biomass increment ? A case study in European beech. *Canadian Journal of Forest Research*, **35**, 2920–2933.

Bradford JB, Kastendick DN (2010) Age-related patterns of forest complexity and carbon storage in pine and aspen–birch ecosystems of northern Minnesota, USA. *Canadian Journal of Forest Research*, **40**, 401–409.

Bunn AG (2008) A dendrochronology program library in R (dplR). *Dendrochronologia*, **26**, 115–124.

Burnham KP, Anderson DR (2002) Model Selection and Multimodel Inference: a Practical Information-Theoretic Approach. Springer Science Business Media Inc., New York, NY, USA.

Canham CD, Lepage PT, Coates KD (2004) A neighborhood analysis of canopy tree competition : effects of shading versus crowding. *Canadian Journal of Forest Research*, **787**, 778–787.

Carrer M (2011) Individualistic and Time-Varying Tree-Ring growth to climate sensitivity. *PLoS ONE*, **6**.

Catovsky S, Holbrook NM, Bazzaz F a (2002) Coupling whole-tree transpiration and canopy photosynthesis in coniferous and broad-leaved tree species. *Canadian Journal of Forest Research*, **32**, 295–309.

Chapin FS, III, Schulze E, Mooney H a (1990) The Ecology and Economics of Storage in Plants. *Annual Review of Ecology and Systematics*, **21**, 423–447.

Clark D, Brown S, Kicklighter DW, Chambers JQ, Thomlinson JR, Ni J (2001) Measuring net primary production in forests: concepts and field methods. *Ecological Applications*, **11**, 356–370.

Cook ER (1987) The Decomposition of Tree-Ring Series for Environmental Studies. *Tree Ring Bulletin*, **47**, 37–58.

Cook ER, Jacoby GC (1977) Tree-Ring-Drought Relationships in the Hudson Valley, New York. *Science*, **198**, 399–401.

Cook ER, Cole J (1991) On predicting the response of forests in eastern North America to future climatic change. *Climatic Change*, **19**, 271–282.

Conkey LE (1979) Response of tree-ring density to climate in Maine, U.S.A. *Tree Ring Bulletin*, **39**, 29–38.

Cronan CS (2003) Belowground biomass, production , and carbon cycling in mature Norway spruce , Maine , U.S.A. *Canadian Journal of Forest Research*, **33**, 339–350.

Cuny HE, Rathgeber CBK, Frank D et al. (2015) Woody biomass production lags stem-girth increase by over one month in coniferous forests. *Nature Plants*, **1**, 1–6.

D'Amato AW, Puettmann KJ (2004) The relative dominance hypothesis explains interaction dynamics in mixed species Alnus rubra / Pseudotsuga menziesii stands. *Journal of Ecology*, **92**, 450–463.

D'Amato AW, Bradford JB, Fraver S, Palik BJ (2011) Forest management for mitigation and adaptation to climate change: Insights from long-term silviculture experiments. *Forest Ecology and Management*, **262**, 803–816.

D'Amato AW, Bradford JB, Fraver S, Palik BJ (2013) Effects of thinning on drought vulnerability and climate response in north temperate forest ecosystems. *Ecological Applications*, **23**, 1735–1742.

Davidson EA, Savage K, Verchot L V, Navarro R (2002) Minimizing artifacts and biases in chamber-based measurements of soil respiration. *Agricultural and Forest Meteorology*, **113**, 21–37.

Day ME (2000) Influence of temperature and leaf-to-air vapor pressure deficit on net photosynthesis and stomatal conductance in red spruce (Picea rubens). *Tree Physiology*, **20**, 57–63.

Daly C, Halbleib M, Smith JI, Gibson WP, Doggett MK, Taylor GH, Curtis J, Pasteris PP (2008) Physiographically sensitive mapping of climatological temperature and precipitation across the conterminous United States. *International Journal of Climatology*, **28**, 2031–2064.

Das A (2012) The effect of size and competition on tree growth rate in old-growth coniferous forests. *Canadian Journal of Forest Research*, **42**, 1983–1995.

Delpierre N, Berveiller D, Granda E, Dufrêne E (2016) Wood phenology, not carbon input , controls the interannual variability of wood growth in a temperate oak forest. *New Phytologist*, **210**, 459–470.

Deslauriers A, Morin H, Begin Y (2003) Cellular phenology of annual ring formation of Abies balsamea in the Quebec boreal forest (Canada). *Canadian Journal of Forest Research*, **200**, 190–200.

Dietze MC, Sala A, Carbone MS, Czimczik CI, Mantooth JA, Richardson AD, Vargas R (2014) Nonstructural Carbon in Woody Plants. *Annual Review of Plant Biology*, **65**, 667–687.

Dixon GE, Keyser CE (2011) Northeast (NE) variant overview: forest vegetation simulator. U.S. Department of Agriculture, Forest Service, Forest Service Management Service Center, Fort Collins.

Drobyshev I, Gewehr S, Berninger F, Bergeron Y (2013) Species specific growth responses of black spruce and trembling aspen may enhance resilience of boreal forest to climate change. *Journal of Ecology*, **101**, 231–242.

Duchesne L, Houle D, Orangeville LD (2012) Influence of climate on seasonal patterns of stem increment of balsam fir in a boreal forest of Québec, Canada. *Agricultural and Forest Meteorology*, **162**–**163**, 108–114.

Dymond CC, Tedder S, Spittlehouse DL, Raymer B, Hopkins K, Mccallion K, Sandland J (2014) Diversifying managed forests to increase resilience. *Canadian Journal of Forest Research*, **44**, 1196–1205.

Eglin T, Francois C, Michelot A, Delpierre N, Damesin C (2010) Linking intra-seasonal variations in climate and tree-ring ^{13}C: A functional modelling approach. *Ecological Modelling*, **221**, 1779–1797.

Epron D, Bahn M, Derrien D et al. (2012) Pulse-labelling trees to study carbon allocation dynamics : a review of methods, current knowledge and future prospects. *Tree physiology*, **32**, 776–798.

Fahey TJ, Siccama TG, Driscoll CT et al. (2005) The Biogeochemistry of Carbon at Hubbard Brook. *Biogeochemistry*, **75**, 109–176.

Fajvan M, Seymour R (1993) Canopy stratification, age structure, and development of multicohort stands of eastern white pine, eastern hemlock, and red spruce. *Canadian Journal of Forest Research*, **23**, 1799–1809.

Finér L, Ohashi M, Noguchi K, Hirano Y (2011) Fine root production and turnover in forest ecosystems in relation to stand and environmental characteristics. *Forest Ecology and Management*, **262**, 2008–2023.

Foster JR, D'Amato AW, Bradford JB (2014) Looking for age-related growth decline in natural forests: Unexpected biomass patterns from tree rings and simulated mortality. *Oecologia*, **175**, 363–374.

Foster JR, Finley AO, D'amato AW, Bradford JB, Banerjee S (2016) Predicting tree biomass growth in the temperate-boreal ecotone: is tree size, age, competition or climate response most important? *Global Change Biology*, 1–13.

Fraver S, White AS (2005) Disturbance dynamics of old-growth Picea rubens forests of northern Maine. *Journal of Vegetation Science*, 597–610.

Fraver S, White AS, Seymour RS (2009) Natural disturbance in an old-growth landscape of northern Maine, USA. *Journal of Ecology*, **97**, 289–298.

Fraver S, D'Amato AW, Bradford JB, Jonsson BG, Mari J, Esseen P (2013) Tree growth and competition in an old-growth Picea abies forest of boreal Sweden : influence of tree spatial patterning. *Journal of Vegetation Science*, 1–12.

Friedrichs DA, Trouet V, Büntgen U, Frank DC, Esper J, Neuwirth B, Löffler J (2009) Species-specific climate sensitivity of tree growth in Central-West Germany. *Trees*, **23**, 729–739.

Frelich LE (2002) Forest dynamics and disturbance regimes. Cambridge University Press, Cambridge, UK.

Fritts HC (1976) Tree Rings and Climate. Academic Press, London, UK.

Gewehr S, Drobyshev I, Berninger F, Bergeron Y (2014) Soil characteristics mediate the distribution and response of boreal trees to climatic variability. *Canadian Journal of Forest Research*, **44**, 487–498.

Girardin MP, Hogg EH, Bernier PY, Kurz WA, Guo XJ, Cyr G (2015) Negative impacts of high temperatures on growth of black spruce forests intensify with the anticipated climate warming. *Global Change Biology*, **22**, 627–643.

Gough CM, Vogel CS, Schmid HP, Su H-B, Curtis PS (2008) Multi-year convergence of biometric and meteorological estimates of forest carbon storage. *Agricultural and Forest Meteorology*, **148**, 158–170.

Gough CM, Flower CE, Vogel CS, Dragoni D, Curtis PS (2009) Whole-ecosystem labile carbon production in a north temperate deciduous forest. *Agricultural and Forest Meteorology*, **149**, 1531–1540.

Goulden ML, Munger JW, Fan S, Daube BC, Wofsy SC (1996) Measurements of carbon sequestration eddy covariance: methods and a critical accuracy by long-term evaluation of accuracy. *Global Change Biology*, **2**, 169–182.

Grace J (2004) Understanding and managing the global carbon cycle. *Journal of Ecology*, **92**, 189–202.

Grant RF, Barr a. G, Black T a. et al. (2009) Interannual variation in net ecosystem productivity of Canadian forests as affected by regional weather patterns - A Fluxnet-Canada synthesis. *Agricultural and Forest Meteorology*, **149**, 2022–2039.

Hargreaves GH, Samani ZA (1982) Estimating potential evapotranspiration. Journal of the Irrigation and Drainage Division, **108**, 225–230.

Harmon M (2001) Carbon sequestration in forests: addressing the scale question. *Journal of Forestry*, **April**, 24–29.

Hartmann H, Trumbore S (2016) Understanding the roles of nonstructural carbohydrates in forest trees – from what we can measure to what we want to know. *New Phytologist*, **211**, 386–403.

Hegyi F (1974) A simulation model for managing jack-pine stands. In: Fries, J. (ed.) *Growth models for tree and stand simulations*, pp. 74–90, Royal College of Forestry, Research Notes 30, Uppsala, SE.

Hendrick RL, Pregitzer KS (1993) The dynamics of fine root length, biomass, and nitrogen content in two northern hardwood ecosystems. *Canadian Journal of Forest Research*, **23**, 2507–2520.

Hennessey TC, Dougherty PM, Cregg B, Wittwer RF (1992) Annual variation in needle fall of a loblolly pine stand in relation to climate and stand density. *Forest Ecology and Management*, **51**, 329–338.

Hicke JA, Allen CD, Desai AR et al. (2012) Effects of biotic disturbances on forest carbon cycling in the United States and Canada. *Global Change Biology*, **18**, 7–34.

Hollinger DY, Goltz SM, Davidson EA, Lee JT, Tu K, Valentine HT (1999) Seasonal patterns and environmental control of carbon dioxide and water vapour exchange in an ecotonal boreal forest. *Global Change Biology*, **5**, 891–902.

Hollinger DY, Aber J, Dail B et al. (2004) Spatial and temporal variability in forest-atmosphere CO2 exchange. *Global Change Biology*, **10**, 1689–1706.

Holmes RL (1983) Computer-assisted quality control in tree-ring dating and measurements. *Tree-Ring Bulletin*, **44**, 69–75.

Honer, TG (1967) Standard volume tables and merchantable conversion factors for the commercial tree species of central and eastern Canada. Canadian Department of Forestry Rural Development, Forest Management Research and Services Institute Information Report FMR-X-5.

Isbell F, Craven D, Connolly J et al. (2015) Biodiversity increases the resistance of ecosystem productivity to climate extremes. *Nature*, **526**, 574–577.

Iverson LR, Prasad AM (1998) Predicting Abundance of 80 Tree Species Following Climate Change in the Eastern United States. *Ecological Monographs*, **68**, 465.

Iverson L, Prasad A, Matthews S (2008) Modeling potential climate change impacts on the trees of the northeastern United States. *Mitigation and Adaptation Strategies for Global Change*, **13**, 487–516.

Johnson SE, Abrams MD (2009) Age class, longevity and growth rate relationships: Protracted growth increases in old trees in the eastern United States. *Tree Physiology*, **29**, 1317–1328.

Kariuki M (2002) Height estimation in complete stem analysis using annual radial growth measurements. *Forestry*, **75**, 63–74.

Keel SG, Siegwolf RTW, Körner C (2006) Canopy CO_2 enrichment permits tracing the fate of recently assimilated carbon in a mature deciduous forest. *New Phytologist*, **172**, 319–329.

Keenan TF, Gray J, Friedl MA et al. (2014) Net carbon uptake has increased through warming-induced changes in temperate forest phenology. *Nature Climate Change*, **4**, 598–604.

Kipfmueller KF, Elliott GP, Larson ER, Salzer W (2010) An Assessment of the Dendroclimatic Potential of Three Conifer Species in Northern Minnesota. *Tree-Ring Research*, **66**, 113–126.

Körner C (2003) Carbon limitation in trees. *Journal of Ecology*, **91**, 4–17.

Körner C (2015) Paradigm shift in plant growth control. *Current Opinion in Plant Biology*, **25**, 107–114.

Kozlowski TT (1992) Carbohydrate Sources and Sinks in Woody Plants. *Botanical Review*, **58**, 107–222.

Kuptz D, Fleischmann F, Matyssek R, Grams TEE (2011) Seasonal patterns of carbon allocation to respiratory pools in 60-yr-old deciduous (*Fagus sylvatica*) and evergreen (*Picea abies*) trees assessed via whole-tree stable carbon isotope labeling. *New Phytologist*, **191**, 160–172.

Lamlom SH, Savidge RA (2003) A reassessment of carbon content in wood: Variation within and between 41 North American species. *Biomass and Bioenergy*, **25**, 381–388.

Lara A, Villalba R (1993) A 3620-year temperature record from *Fitzroya cupressoides* tree rings in southern South America. *Science*, **260**, 1104–1104.

Lara W, Bravo F, Maguire DA (2013) Modeling patterns between drought and tree biomass growth from dendrochronological data : A multilevel approach. *Agricultural and Forest Meteorology*, **178**–**179**, 140–151.

Law BE, Sun OJ, Campbell J, Van Tuyl S, Thornton PE (2003) Changes in carbon storage and fluxes in a chronosequence of ponderosa pine. *Global Change Biology*, **9**, 510–524.

Li R, Weiskittel A, Dick AR, Kershaw J a., Seymour RS (2012) Regional Stem Taper Equations for Eleven Conifer Species in the Acadian Region of North America: Development and Assessment. *Northern Journal of Applied Forestry*, **29**, 5–14.

Lorimer CG, Dahir SE, Nordheim E V (2001) Tree mortality rates and longevity in mature and old-growth hemlock-hardwood forests. *Journal of Ecology*, **89**, 960–971.

Luyssaert S, Schulze E-D, Börner A et al. (2008) Old-growth forests as global carbon sinks. *Nature*, **455**, 213–5.

Malmsheimer R, Heffernan P, Brink S et al. (2008) Forest management solutions for mitigating climate change in the United States. *Journal of Forestry*, **April/May**, 115–173.

Martín-Benito D, Cherubini P, Del Río M, Cañellas I (2008) Growth response to climate and drought in *Pinus nigra* Arn. trees of different crown classes. *Trees*, **22**, 363-373.

Menne MJ, Durre I, Vose RS, Gleason BE, Houston TG, (2012) An overview of the Global Historical Climatology Network-Daily database. *Journal of Atmospheric and Oceanic Technology*, **29**, 897–910.

Mérian P, Lebourgeois F (2011) Size-mediated climate-growth relationships in temperate forests: A multi-species analysis. *Forest Ecology and Management*, **261**, 1382–1391.

Michelot A, Eglin T, Dufrêne E, Lelarge-Trouverie C, Damesin C (2011) Comparison of seasonal variations in water-use efficiency calculated from the carbon isotope

composition of tree rings and flux data in a temperate forest. *Plant, Cell and Environment*, **34**, 230–244.

Millar CI, Stephenson NL, Stephens SL (2007) Climate Change and Forests of the Future: Managing in the Face of Uncertainty. *Ecological Applications*, **17**, 2145–2151.

Miles PD, Smith BW (2009) Specific gravity and other properties of wood and bark for 156 tree species found in North America. U.S. Department of Agriculture, Forest Service, Northern Research Station. Research Note NRS-38, 35p.

Miyamoto Y, Griesbauer HP, Green DS (2010) Growth responses of three coexisting conifer species to climate across wide geographic and climate ranges in Yukon and British Columbia. *Forest Ecology and Management*, **259**, 514–523.

Mohan JE, Cox RM, Iverson LR (2009) Composition and carbon dynamics of forests in northeastern North America in a future, warmer world. *Canadian Journal of Forest Research*, **39**, 213–230.

Morin X, Lechowicz M, Augspurger C, O'Keefe J, Viner D, Chuine I (2009) Leaf phenology in 22 North American tree species during the 21st century. *Global Change Biology*, **15**, 961–975.

Moores AR, Seymour RS, Kenefic LS (2007) Height development of shade-tolerant conifer saplings in multiaged Acadian forest stands. *Canadian Journal of Forest Research*, **37**, 2715–2723.

Moreira X, Abdala-Roberts L, Linhart YB, Mooney KA (2015) Effects of climate on reproductive investment in a masting species : assessment of climatic predictors and underlying mechanisms. *Journal of Ecology*, **103**, 1317–1324.

Naeem S, Li S (1997) Biodiversity enhances ecosystem reliability. *Nature*, **390**, 507–509.

Pan Y, Birdsey R, Fang J et al. (2011) A large and persistent carbon sink in the world's forests. *Science*, **333**, 988–994.

Pereira JS, Mateus JA, Aires LM et al. (2007) Net ecosystem carbon exchange in three contrasting Mediterranean ecosystems – the effect of drought. *Biogeosciences*, **4**, 791–802.

Polgar C a, Primack RB (2011) Leaf-out phenology of temperate woody plants: from trees to ecosystems. *The New phytologist*, **191**, 926–41.

Pregitzer KS, Euskirchen ES (2004) Carbon cycling and storage in world forests: biome patterns related to forest age. *Global Change Biology*, **10**, 2052–2077.

Ranson K., Sun G, Knox R., Levine E., Weishampel J., Fifer S. (2001) Northern Forest Ecosystem Dynamics Using Coupled Models and Remote Sensing. *Remote Sensing of Environment*, **75**, 291–302.

Richardson AD, Hollinger DY, Dail DB, Lee JT, Munger JW, O'keefe J (2009) Influence of spring phenology on seasonal and annual carbon balance in two contrasting New England forests. *Tree physiology*, **29**, 321–31.

Richardson AD, Williams M, Hollinger DY et al. (2010) Estimating parameters of a forest ecosystem C model with measurements of stocks and fluxes as joint constraints. *Oecologia*, **164**, 25–40.

Richardson AD, Anderson RS, Arain MA et al. (2012) Terrestrial biosphere models need better representation of vegetation phenology : results from the North American Carbon Program Site Synthesis. *Global Change Biology*, **18**, 566–584.

Richardson AD, Carbone MS, Keenan TF et al. (2013) Seasonal dynamics and age of stemwood nonstructural carbohydrates in temperate forest trees. *The New phytologist*, **197**, 850–61.

Rocha A V., Goulden ML, Dunn AL, Wofsy SC (2006) On linking interannual tree ring variability with observations of whole-forest CO2 flux. *Global Change Biology*, **12**, 1378–1389.

Roland CA, Schmidt JH, Johnstone JF (2014) Climate sensitivity of reproduction in a mast-seeding boreal conifer across its distributional range from lowland to treeline forests. *Oecologia*, **174**, 665–677.

Rossi S, Deslauriers A, Anfodillo T et al. (2006) Conifers in cold environments synchronize maximum growth rate of tree-ring formation with day length. *New Phytologist*, **170**, 301–310.

Rossi S, Deslauriers A, Seo J et al. (2008) Critical temperatures for xylogenesis in conifers of cold climates. *Global Ecology and Biogeography*, **17**, 696–707.

Rustad LE (1994) Element Dynamics along a Decay Continuum in a Red Spruce Ecosystem in Maine, USA. *Ecology*, **75**, 867–879.

Ryan MG, Lavigne MB, Gower ST (1997) Annual carbon cost of autotrophic respiration in boreal forest ecosystems in relation to species and climate. *Journal of Geophysical Research*, **102**, 28,871-28,883.

Sánchez-Salguero R, Linares JC, Camarero JJ, et al. (2015) Disentangling the effects of competition and climate on individual tree growth: A retrospective and dynamic approach in Scots pine. *Forest Ecology and Management*, **358**, 12-25.

Seymour RS, Hunter ML, Jr (1992) New forestry in eastern spruce-fir forests: Principles and applications to Maine. Maine Agricultural and Forest Experiment Station Miscellaneous Publication 716.

Sun G, Ranson KJ, Guo Z, Zhang Z, Montesano P, Kimes D (2011) Forest biomass mapping from lidar and radar synergies. *Remote Sensing of Environment*, **115**, 2906–2916.

Stephenson NL, Das AJ, Condit R et al. (2014) Rate of tree carbon accumulation increases continuously with tree size. *Nature*, **507**, 90–3.

Thibeault-Martel M, Krause C, Morin H, Rossi S (2008) Cambial Activity and Intra-annual Xylem Formation in Roots and Stems of Abies balsamea and Picea mariana. *Annals of Botany*, **102**, 667–674.

Thomas CK, Law BE, Irvine J, Martin JG, Pettijohn JC, Davis KJ (2009) Seasonal hydrology explains interannual and seasonal variation in carbon and water exchange in a semiarid mature ponderosa pine forest in central Oregon. *Journal of Geophysical Research*, **114**, 22.

Ueyama M, Kai A, Ichii K, Hamotani K, Kosugi Y, Monji N (2011) The sensitivity of carbon sequestration to harvesting and climate conditions in a temperate cypress forest: Observations and modeling. *Ecological Modelling*, **222**, 3216–3225.

U.S. Geological Survey (2016) National Water Information System data available on the World Wide Web (USGS Water Data for the Nation), accessed 25 April 2016, at URL http://waterdata.usgs.gov/usa/nwis/uv?01034500

Vann DR, Johnson AH, Casper BB (1994) Effect of elevated temperatures on carbon dioxide exchange in Picea rubens. *Tree Physiology*, **19**, 1339–1350.

Walker X, Johnstone JF (2014) Widespread negative correlations between black spruce growth and temperature across topographic moisture gradients in the boreal forest. *Environmental Research Letters*, **9**, 64016.

Weishampel JF, Sung G, Ransom KJ, LeJeune KD, Shugart HH (1994) Forest textural properties from simulated microwave backscatter: The influence of spatial resolution. *Remote Sensing of Environment*, **47**, 120–131.

Wharton S, Falk M (2016) Climate indices strongly influence old-growth forest carbon exchange. *Environmental Research Letters*, **11**, 44016.

Wilmking M, Juday GP, Barber VA, Zald HSJ (2004) Recent climate warming forces contrasting growth responses of white spruce at treeline in Alaska through temperature thresholds. *Global Change Biology*, **10**, 1724–1736.

Young HE, Ribe JH, Wainwright K (1980) Weight tables for tree and shrub species in Maine. University of Maine, Orono, ME, Miscellaneous Report 230.

Zweifel R, Zimmermann L, Zeugin F, Newbery DM (2006) Intra-annual radial growth and water relations of trees : implications towards a growth mechanism. *Journal of Experimental Botany*, **57**, 1445–1459.

Zweifel R, Eugster W, Etzold S, Dobbertin M, Buchmann N, Häsler R (2010) Link between continuous stem radius changes and net ecosystem productivity of a subalpine Norway spruce forest in the Swiss Alps. *The New phytologist*, **187**, 819–30.

APPENDIX: SUPPLEMENTAL INFORMATION

Table A.1: NASA plot stand attributes by species. Data represents the number and size of living trees, trees that died, and ingrowth of trees (≥ 10 cm) between the two sampling periods (1989 and 2015).

Species	Living (tph) 1989	QMD (cm) 1989	Living (tph) 2015	QMD (cm) 2015	Mortality (tph)	Mortality QMD (cm)	Ingrowth (tph)
Red spruce	521.3	19.1	471.3	21.3	98.0	14.4	48
Eastern hemlock	269.9	18.3	293.2	22.1	24.7	15.6	48
White pine	37.2	26.0	51.7	37.5	1.7	22.2	16.2
N. white-cedar	112.8	18.1	113.5	19.8	18.2	15.3	18.9
Red maple	78.0	16.0	94.9	19.3	12.5	14.2	29.4
Balsam fir	14.9	13.7	22	11.8	14.9	16.6	22
Yellow birch	4.1	26.7	4.4	28.5	0	n/a	0.3
Paper birch	5.4	17.7	4.1	20.2	1.4	12.1	0
Stand-level	1043.6	19.0	1055.1	22.1	171.3	14.9	182.8

tph = trees per hectare

QMD= quadratic mean diameter

Table A.2: Species-level carbon mass storage per hectare in the NASA plot living pool using Young's equations (Young et al. 1989). Data represents storage from the initial mapping (1989) and re-measurement (2015), and average annual change.

Species	Living 1989 (kg/ha)	Living 2015 (kg/ha)	Mean CMI* (kg/ha)	Change
Red spruce	34,269.8	44,925.5	409.8	+31%
Eastern hemlock	19,034.1	29,397.3	398.6	+54%
White pine	7,372.4	17,581.8	392.7	+138%
Northern white cedar	4,303.4	5,152.5	32.7	+19%
Red maple	5,876.7	8,910.6	116.7	+52%
Balsam fir	764.6	461.8	-11.6	-40%
Yellow birch	952.3	1,077.7	4.8	+13%
Paper birch	304.9	499.6	7.5	+64%
TOTAL	72,878.2	108,006.9	1,351.1	+48%

*Mean CMI = average annual stand-level carbon mass increment

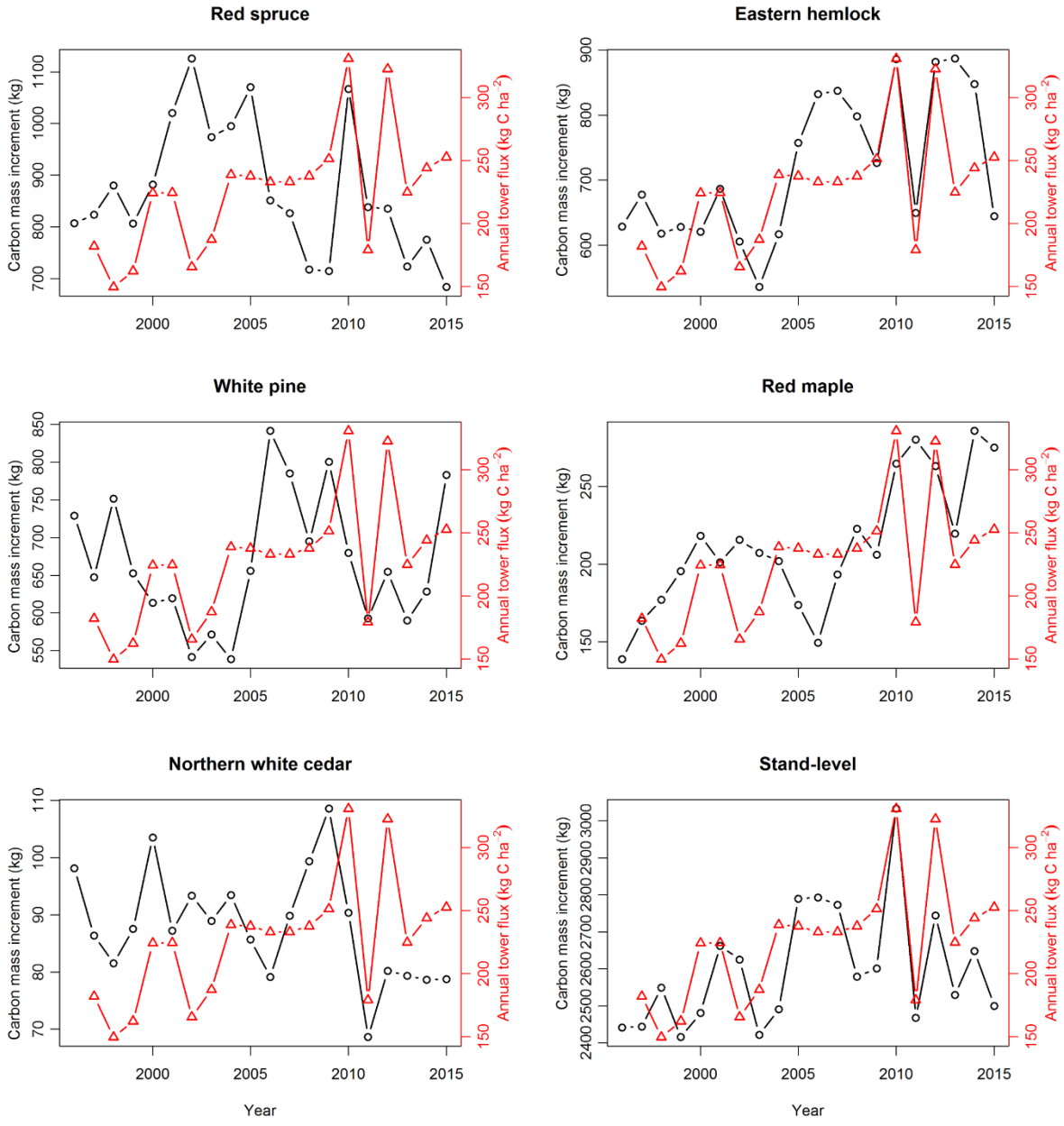

Figure A.1: Comparison of species-level carbon mass increment (derived from tree-ring series) and shifted annual carbon flux (eddy flux data) from previous year September to following September.

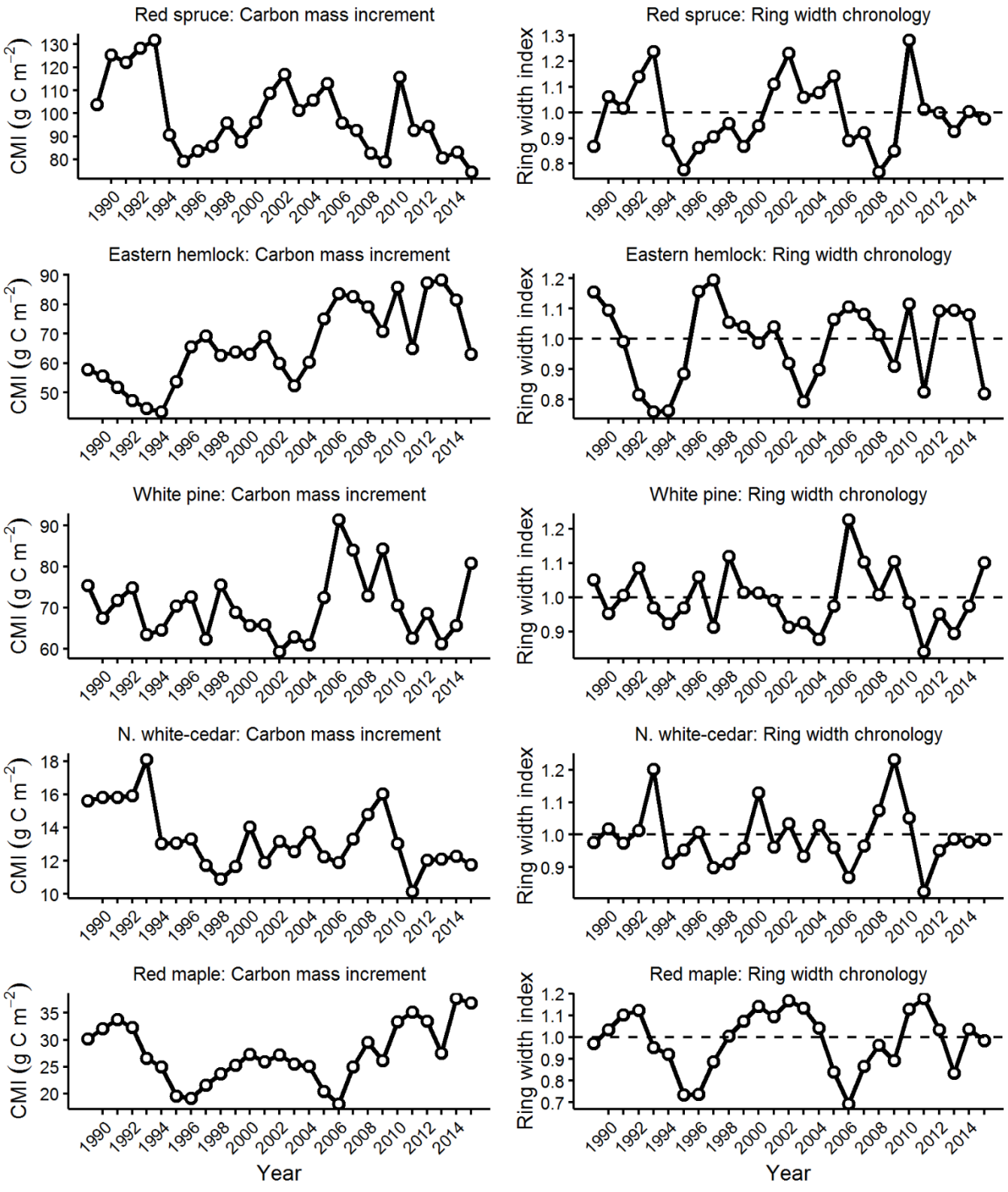

Figure A.2: Cumulative carbon mass increment (left column) compared to dimensionless tree-ring chronology (right column) plotted by species.

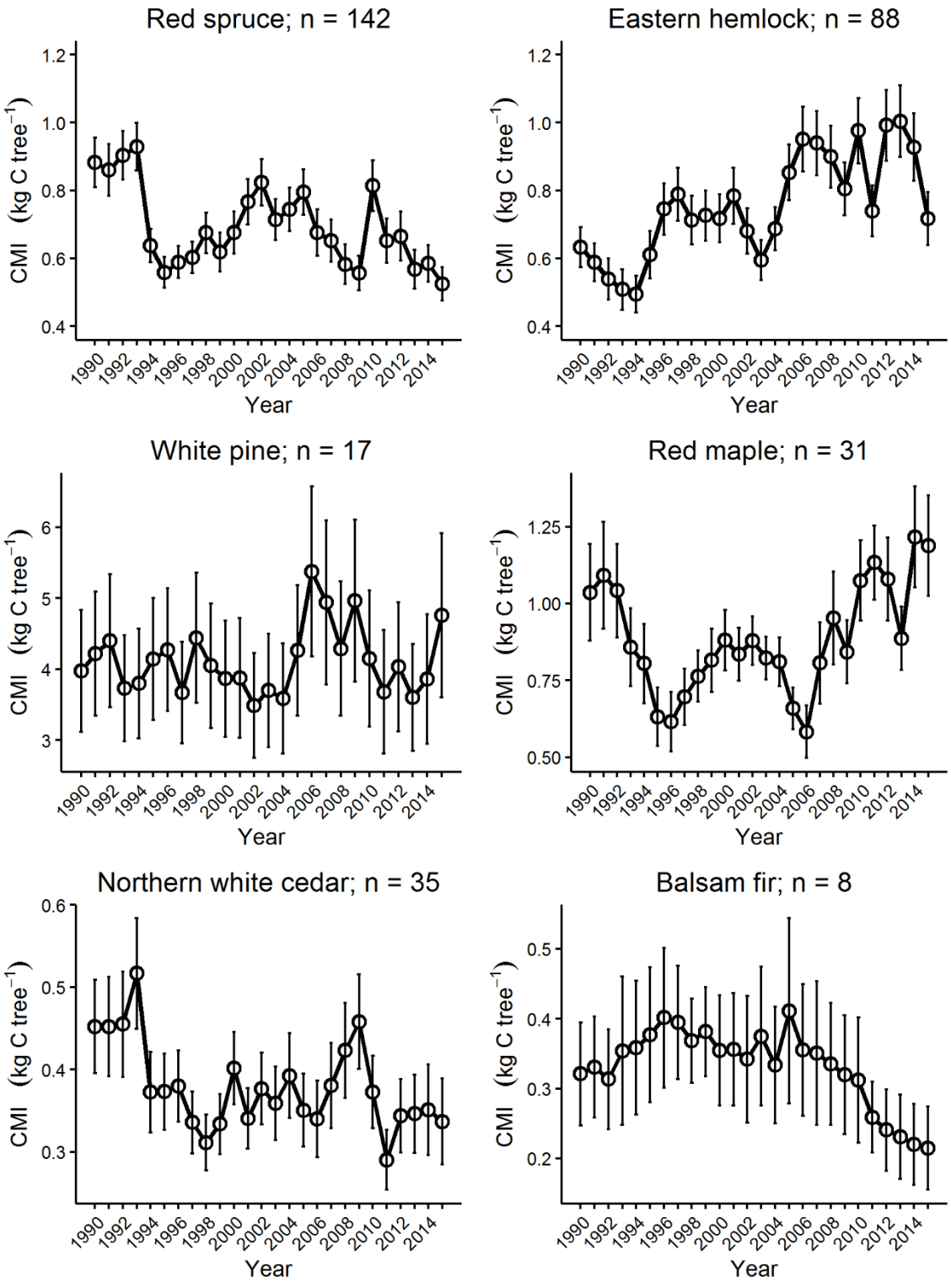

Figure A.3: Annual variability in species-level growth. The carbon mass increment (CMI) from the six most common species are presented. The error bars represent the standard error, and n is the number of trees used for each summary.

Table A.3: Summary of tree-level carbon mass increment (CMI) by species. Reported mass change (kg) in individual tree boles were calculated using the Honer (1967) volume equation.

Species	Average bole C mass	Average CMI	CMI SD*	Maximum CMI	Minimum CMI
Red spruce	52.3	0.7	0.7	6.5	0.0
Eastern hemlock	49.5	0.8	0.7	4.5	0.0
White pine	163.2	4.1	3.7	17.4	0.0
Northern white-cedar	29.6	0.4	0.3	1.8	0.0
Red maple	56.4	0.9	0.7	4.5	0.0
Balsam fir	7.4	0.3	0.2	1.3	0.0

*CMI SD = standard deviation of carbon mass increment

Table A.4: Species-level response function analysis summary for standardized tree-ring chronologies (n=number of trees). The prefix *p* indicates previous year variable.

	n	tmax	tmean	tmin	gdd	precip	snow	P/PET	cfs
Red spruce	142	-pJUL	-pJUL	-pJUL	-pJUL, +AUG	-	-	-	-
Eastern hemlock	88	+JAN +FEB	+FEB	-	-	+pJUN +FEB +APR	-	+MAY	-
White pine	17	-	+MAY	-	+MAY	+pJUL	-	-pDEC	-MAR
N. white-cedar	37	-JUL	+APR	-	-	-	-	-	-
Red maple	31	+pMAY MAY	-	+AUG	+pMAY	-MAY	-	-MAY	-

BIOGRAPHY OF THE AUTHOR

Aaron Teets was born in Rockville, Maryland and graduated from Middletown High School (Middletown, MD) in 2004. He attended Virginia Tech, and graduated cum laude in May, 2008 with a degree in Biological Sciences. Following his undergraduate degree, Aaron was employed by a department of College of Natural Resources at Virginia Tech (the Conservation Management Institute) from 2008-2014 where he became a field-crew leader and project assistant for various natural resources related grants. Aaron's interest in carbon dynamics began through his involvement with several Reduced Emissions from Deforestation and Degradation (REDD+) projects, which required quantifying carbon stocks in backcountry areas of Belize and Peru. Carbon projects ultimately led him to the University of Maine where he pursued carbon-cycle research under the guidance of Dr. Shawn Fraver. He served as the President of the Forestry Graduate Student Club in the 2015-2016 school year, where he focused on strengthening relationships between graduate students in the School of Forest Resources. He is a co-author of a research note in *Northeastern Naturalist* involving climate response of Pitch pine (*Pinus rigida*) at Acadia National Park, scheduled to be printed in 2017. Aaron is a candidate for the Master of Science degree in Forest Resources from the University of Maine in December 2016.